Jun 2016

The Swan-Canning

Estuarine Response Model

(SCERM) v1

Model Science Basis and Parameterisation

AED
Aquatic Eco Dynamics

Department of **Parks and Wildlife**

SWAN CANNING RIVERPARK

THE UNIVERSITY OF **WESTERN AUSTRALIA**
SEEK WISDOM

Government of Western Australia
Department of **Water**

Executive Summary

The Swan-Canning estuary is an iconic waterway of Western Australia and supports multiple ecosystem services vital to the Perth community. Eutrophication is a major issue facing this waterway, with complex interactions between nutrient and organic loading, algal blooms, water chemistry and hydrodynamic changes affected by climate. The sustainable management of the estuary requires a holistic view of its ability to respond to multiple stressors over both the short and long-term, and the potential for strategic development of an "**Estuarine Response Model**" platform has been identified as necessary to assist decision-making and assess management initiatives.

Whilst several modelling efforts have been undertaken in the past which have provided important insights into the drivers of various aspects of water quality, to date these have either had a short-term focus or low level of predictability in terms of the priority needs of management agencies. The aim of this document is to develop a consensus view of the most appropriate level of model complexity and parameterisation approach based on a review of past literature and consideration of available data for model setup and validation. This summary forms the basis of the recent 3D model developed by The University of Western Australia and Department of Water for the River and Estuaries Division of the Department of Parks and Wildlife.

This document firstly sets the context and defines the need for a decision support tool, and secondly provides a technical summary of approaches to simulate turbidity, oxygen, nutrient cycling, sediment biogeochemistry, phytoplankton and seagrass. Appropriate parameterisations and parameter values relevant to the Swan-Canning are also discussed and summarised. These parameters have been used as the basis for current model development work being undertaken within the AED2 water quality modelling platform on the SCE and the validation of the model is presented in an accompanying report. A further section is included to identify future development priorities for aspects that are currently at the limit of our modelling ability.

CONTRIBUTORS

Matthew R Hipsey [a]
Kieryn Kilminster [b]
Samuel Robinson [c]
Alice Gedaria [b]
Kerry Trayler [d]

[a] Aquatic Ecodynamics, School of Earth and Environment, The University of Western Australia, Crawley WA 6009, Australia.

[b] Water Science Branch, Department of Water, Perth WA 6842, Australia.

[c] Centre for Fish and Fisheries Research, Murdoch University, Murdoch WA 6150, Australia.

[d] Rivers and Estuaries Division, Department of Parks and Wildlife, Bentley WA 6983, Australia.

ACKNOWLEDGEMENTS

REVISION AND DISTRIBUTION HISTORY

Issue	Issued to	Qty	Date	Reviewed	Approved
V1 (prelim)	*Swan Modelling Working Group*	e	*17 May 2015*	-	
V3	*Kerry Trayler*	e	*10 Apr 2016*	*K Trayler*	
V4	*Swan Modelling Working Group*		*10 Jun 2016*	*K Kiliminster M Hipsey*	

RELEASE STATUS:

Confidential: No

FINAL

DOCUMENT DETAILS

Contents

1. Introduction & Objectives

The Swan-Canning estuary is an iconic waterway of Western Australia and supports multiple ecosystem services vital to the Perth community. Eutrophication is a major issue facing the system, with complex interactions between nutrient and organic loading, algal blooms, water chemistry and hydrodynamic variability as impacted by the drying trend in climate.

Excess nutrients and organic matter arising from the urban and rural landscape drive nuisance and toxic algal blooms in the waterway and contribute to low oxygen conditions in the upper reaches of the Swan and Canning. These impact on fish and other aquatic organisms. Non-nutrient contaminants such as metals, pesticides and hydrocarbons have also found their way into the river system and persist in sediments. The effects of a drying climate, such as reduced rainfall and stream flow increase the rivers' vulnerability to oxygen depletion, nutrient enrichment and other biodiversity threats. The Healthy Rivers Action Plan (HRAP) was released by the Swan River Trust in 2008 as a 5-year, $40 million plan to protect the environmental health and community benefit of the Swan and Canning rivers by improving water quality. In particular, the HRAP and subsequent initiatives undertaken by relevant stakeholders have introduced numerous management interventions to reduce nutrient, sediment and contaminant loads to the main estuary, oxgyenate the upstream reaches of the system, and to restore and protect riparian and fringing vegetation and associated habitat. These interventions have been demonstrated to have a positive impact, for example, drainage nutrient intervention (Ruibal-Conti et al., 2015; Adyel et al., 2015) and artificial oxygenation (Hipsey et al., 2013) to name a few. The current Swan Canning River Protection Strategy (Dept Parks and Wildlife, 2015) aims to achieve long-term sustainable management strategies and identifies the priority objectives for a healthy waterway as:

- Improved water quality and managed environmental flow
- Ensuring management decisions are based on appropriate knowledge
- Protected, managed and enhanced biodiversity"

This requires a holistic view of estuarine response to multiple stressors over both the short and long-term. The development and application of integrated models has advanced to support decision making in this regard, for example in identifying nutrient reduction targets (Kim et al., 2014; Waltham et al., 2014), controls on harmful algal blooms (Chung et al., 2014; Robson and Hamilton, 2004), and identifying public health risks (Hipsey et al., 2008). Previously within the Swan-Canning system, prior efforts to develop hydrodynamic-biogeochemical models have been reported by (Chan et al., 2002; Robson and Hamilton, 2004; Vilhena, 2013; Hipsey et al., 2013). Whilst these have provided important insights into the drivers of various aspects of water quality, to date these have either had a short-term focus or low level of predictability in terms of the priority management areas defined above.

It has been identified that the strategic development of an "**Estuarine Response Model**" for the Swan-Canning system that is able to support decision making related to the management challenges identified above, could help build a holistic picture of the system. By integrating various field investigations and the extensive long-term monitoring data, such a system offer the potential to synthesize our knowledge of the estuarine function across a broad range of disciplines and spatio-temporal scales. Ultimately such a system would also be suited to undertake forecast predications of the long-term system response to ongoing land-use and climate change and to identify thresholds of change and the level of resilience.

However, whilst there are various platforms available for estuarine modelling and successful examples of model applications, including San Francisco Bay (Cloern et al., 2011), Chesapeake Bay (Testa et al., 2014), and the Derwent estuary (Wild-Allen et al., 2013), setting up models to address multiple attributes relevant to ecosystem "health" is notoriously challenging. This is due to uncertainties in parameterising key process pathways, accommodating spatial-temporal variability in sediment properties and boundary conditions, and inadequate monitoring data to fully constrain model predictions. In cases where these issues are not appropriately addressed then often model predictions may not meet their intended objectives and have limited utility to meaningfully support management.

The aim of developing this document was to develop a consensus view of the most appropriate model complexity and parameterisation approach through review of past literature and consideration of available data for model setup and validation. A further section is included to identify future development priorities for aspects that are currently at the limit of our modelling ability but of interest for model development activities and ongoing research. An accompanying validation report is also available describing performance of v1 of the Swan Canning Estuarine Response Model, as assessed against historical monitoring data, based on the setup and parameterisation described herein (Hipsey et al., 2016a).

2. Modelling scope and prior modelling efforts

There are a wide range of attributes of relevance to estuary health that have been the focus of prior modelling studies. In general terms, there have been substantial advances in application of hydrodynamic models to estuaries across Australia with a substantially lower number of studies focused on modelling water quality and estuarine ecology. A non-exhaustive list of contemporary applications occurring within Australia include:

- LI: Leschenault Inlet.   - Gillibrand *et al.*, 2012
- MB: Moreton Bay.   - Herzfeld *et al.*, 2014
- SEQ: SE Queensland estuaries.   - BMTWBM (2016), Adiyanti et al. (2016)
- CLL: Coorong, Lower Lakes and Murray Mouth.   - Hipsey et al. (2014b); Hipsey and Busch (2012)
- YE: Yarra River estuary.   - Bruce et al. (2014), Bruce et al. (2015)
- GL. Gippsland Lakes.   - Zhu et al. (2016)
- DE: Derwent Estuary.   - Wild-Allen et al. (2013)
- HN: Hawkesbury-Nepean River.   - BMTWBM (2014)
- BB: Botany Bay.   - Lee and Birch (2012)
- CB: Collier Bay & Walcott Inlet.   - Bruce et al. (2016)
- FR: Fitzroy River.   - Robson et al. (2006)

Table 1 summarises these applications with an indicative assessment of the level of detail addressed within seven categories, ranging from hydrodynamics to system trajectories. Within each category, a range of development areas have been arbitrarily defined considering different aspects of the model setup process.

Focusing on the Swan-Canning system, several prior modelling studies have occurred (e.g., Chan et al., 2002; Hipsey et al., 2014a; Vilhena, 2013; Marti et al., 2015). Based on an assessment of the current capability reported in relevant publications, Table 2 summarises the current state of prediction ability for 3 sub-regions of the system:

1. Lower Swan-Canning Estuary   - *Narrows & Kent St > Fremantle*
2. Upper Swan River – *Gt Northern Hwy > Narrows*
3. Canning Weir Pool – *Canning River & Southern River > Kent St*

Whilst there is a range of ongoing activities relevant to model development, the tables highlight substantial effort is required to further build capacity to make robust predictions for many aspects relevant to the simulation of estuarine health.

The remainder of this Science Plan document scopes out the approach for building a Swan-Canning Estuarine Response Model (SCERM), within the "AED" open-source model framework. However, many of the parameterisations and review undertaken in the subsequent sections is described generally, and is based on work undertaken with or able to be implemented within alternative model platforms (e.g., ROMS-BGC, CSIRO-EMS, DELFT3D-WAQ, ELCOM-CAEDYM, MIKE3-EcoLab etc). The AED source code is available as part of the Framework for Aquatic Biogeochemical Models (FABM; Bruggeman and Bolding, 2014), or may be coupled directly to hydrodynamics models as part of the AED2 package.

Scope for development of a comprehensive biogeochemical model

Based on prior experience and known data limitations, a model schematic relevant to the Swan-Canning estuary is summarised in Figure 1. The model captures oxygen, suspended sediment and inorganic nutrients, several organic matter groups, phytoplankton functional groups and benthic biotic components. Variable descriptions and relevant processes are summarised in Table 3.

Table 1. Overview of modelling activity within Australian estuaries, categorised based on seven model focus areas.

Model Development Focus	LI	MB	SEQ	CLL	YE	GL	DE	HN	BB	WI
Hydrodynamics										
• Tidal Propagation & Wetting/Drying	+++	+++	+++	+++	+++	+++	+++	+++	+++	+++
• Salt-Wedge & Mixing	+	++	++	++	+++	++	++	++	+	++
• Surface Thermodynamics	++	++	++	++	+++	++	+++	++	?	++
• Erosion / Deposition	-	++	++	++	-	++	++	++	-	+
Oxygen										
• Anoxia/Hypoxia	-	+	+	++	+++	++	++	++	-	+
• Oxygenation	n/a	n/a	n/a	n/a	n/a	n/a	n/a	n/a	n/a	n/a
Nutrients & Sediment										
• Dissolved Nutrients	-	++	++	++	+++	++	+++	++	-	+++
• Organic Matter Dynamics	-	+	+++	++	++	++	++	++	+	++
• PO_4 Sorption	-	-	+	+	-	+	-	+	-	+
• N_2 Fixation & Denitrification	-	+	+	+	++	++	++	+	-	+
• Light Climate & Turbidity	-	+	++	++	+	+	++	++	-	+++
• CO_2 exchange & DIC/pH	-	++	++	++	-	-	++	++	-	-
• C & N isotope data	-	-	+++	-	+	-	-	-	+	+
• Sediment Biogeochemistry	-	++	+	++	+	++	+	+	-	+
• Sediment Zones	-	++	+	++	-	+	+	+	-	+
• Sediment Redistribution	-	+++	++	-	-	-	+	++	-	+
• Tributary Loading Estimates	-	++	++	++	++	++	++	++	-	+
• Groundwater Seepage & Riparian Connectivity	-	-	-	+++	-	-	-	-	-	-
Phytoplankton										
• Community trends	-	++	+	+	-	++	++	+	-	++
• Pico's and Synechococcus	-	+	-	-	-	-	-	-	-	+
• HAB Dynamics (eg, *Karlodinium, Nodularia, Lyngbya*)	-	+	-	-	-	++	+	+	-	-
• Toxin production	-	-	-	-	-	-	-	-	-	-
Zooplankton & Fish										
• Macro Grazers & Copepods	-	++	-	-	-	-	++	-	-	++
• Food Quality & Grazing Rates	-	-	-	-	-	-	-	-	-	-
• Bacteria & Microbial Loop	-	-	-	-	-	-	-	-	-	+
• Jellies	-	-	-	-	-	-	-	-	-	-
• Fish Eggs/Larval Dynamics	-	-	-	-	-	+	-	-	-	-
• Fish Kills	-	-	-	-	-	-	-	-	-	-
Benthos										
• Microphytobenthos	-	+	-	-	-	-	-	-	-	-
• Seagrass & Epiphyton Productivity	-	++	-	-	-	+	-	-	-	-
• Benthic Infauna	-	-	-	-	-	-	-	-	-	-
• Low Oxygen Exposure Limits	-	-	-	-	-	-	-	-	-	-
System Resilience & Response Trajectories										
• Flow-Response Relationships	-	-	-	+	+	-	-	-	-	+
• Nutrient Load Reductions	-	+	-	-	-	+	++	++	-	-
• Benthic Response to Oxygenation	-	-	-	-	-	-	-	-	-	-
• Community Response	-	-	-	-	-	-	-	-	-	-
LEGEND: +++ Excellent model prediction; ++ Satisfactory model prediction; + Less confidence in model prediction; - not modelled ; ~ unclear ; n/a not applicable										

AED

Table 2. Overview of modelling activity within the Swan-Canning estuary, categorised using seven model focus areas.

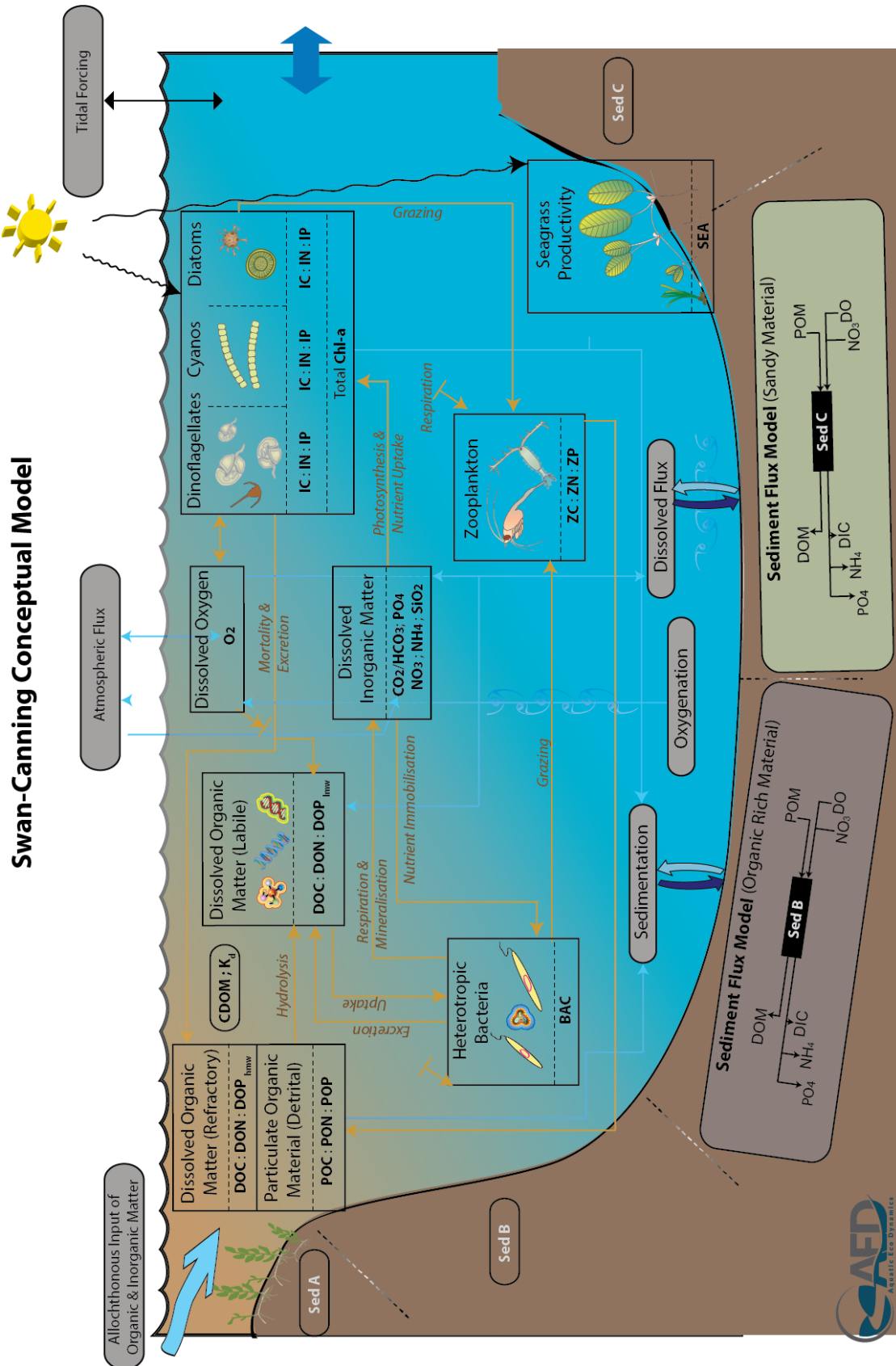| *Model Development Focus*	Region 1 – Lower Estuary	Region 2 – Upper Swan	Region 3 – Kent St Weir Pool	Comments / Next Steps
Hydrodynamics				This has been done well by models like ELCOM and TUFLOW-FV. The salt-wedge in the Upper Swan was well resolved in Hipsey et al (2013) simulations.
• Tidal Propagation & Wetting/Drying	+	+++	++	
• Salt-Wedge & Mixing	+	+++	++	
• Surface Thermodynamics	+	+	+	
• Erosion / Deposition	-	-	-	
Oxygen				Further work on near-field dynamics of the oxygen bubble plume, DO control, and flow variability on plant performance is required
• Anoxia/Hypoxia	~	+++	++	
• Oxygenation	n/a	++	+	
Nutrients				Nutrients have been simulated in the past ELCOM-CAEDYM simulations, but with further effort in validation required to capture the seasonal and spatial gradients.
• Dissolved Nutrients	+	+	+	
• Organic Matter Dynamics	+	~	~	
• PO_4 Sorption	-	-	-	Organic matter could be improved by accounting for CDOM and refractory pools.
• N_2 Fixation & Denitrification	+	+	-	
• Light Climate & Turbidity	+	+	-	Light, turbidity and pH have not been validated.
• CO_2 exchange & DIC/pH	-	-	-	
• C & N isotope data	-	-	-	Sediment diagenetic process were simulated by Norlem et al. (2013), but this was not linked to a water column model
• Sediment Biogeochemistry	-	++	-	
• Sediment Zones	-	-	-	
• Tributary Loading Estimates	+	+	-	
• Groundwater Seepage & Riparian Connectivity	-	-	-	
Phytoplankton				Broad functional groups were simulated by Chan (2006) though this did not account for picoplankton or HAB dynamics specifically. Robson and Hamilton (2004) and Vilhena (2013) simulated HAB dynamics.
• Community trends	++	+	-	
• Pico's and Synechococcus	-	-	-	
• HAB Dynamics (*Karlodinium*)	+	~	-	
Zooplankton & Fish				
• Macro Grazers & Copepods	-	-	-	
• Food Quality & Grazing Rates	-	-	-	
• Bacteria & Microbial Loop	-	-	-	
• Jellyfish	-	-	-	
• Fish Eggs/Larval Dynamics	-	-	-	
• Fish Kills	-	-	-	
Benthos				
• Microphytobenthos	-	-	-	
• Seagrass & Epiphyton Productivity	-	-	-	
• Benthic Infauna	-	-	-	
• Low Oxygen Exposure Limits	-	-	-	
System Response Trajectories				
• Flow-Response Relationships	-	-	-	
• Nutrient Load Reductions	-	-	-	
• Benthic Response to Oxygenation	-	-	-	
• Community Response	-	-	-	
LEGEND: +++ Excellent model prediction; ++ Satisfactory model prediction; + Less confidence in model prediction; - not modelled ; ~ unclear ; n/a not applicable				

Swan-Canning Conceptual Model

Figure 1. Conceptual diagram highlighting key variables and interactions within the model.

Table 3: Relevant variables configurable within the proposed model framework.

Variable	Units *	Common Name	Process Description
Physical variables			
T	°C	Temperature	Temperature modelled by hydrodynamic model, subject to surface heating and cooling processes
S	psu	Salinity	Salinity simulated by the hydrodynamics model, impacting density. Subject to tributary, drain and groundwater inputs, and evapo-concentration
EC	uS cm^{-1}	Electrical conductivity	Derived from salinity and temperature
I$_{PAR}$	mE m^{-2} s^{-1}	Shortwave light intensity	The PAR fraction of incident light, I$_0$, is attenuated as a function of depth
I$_{UV}$	mE m^{-2} s^{-1}	UV light intensity	The UV fraction of incident light, I$_0$, is attenuated as a function of depth
η_{PAR}	m^{-1}	PAR extinction coefficient	Bandwidth specific extinction coefficient computed based on organic matter and suspended material
η_{UV}	m^{-1}	UV extinction coefficient	
Core biogeochemical variables			
DO	mmol O$_2$ m^{-3}	Dissolved oxygen	Impacted by photosynthesis, organic decomposition, nitrification, surface exchange, and sediment oxygen demand
RSi	mmol Si m^{-3}	Reactive Silica	Algal uptake and subsequent sedimentation, sediment flux
FRP	mmol P m^{-3}	Filterable reactive phosphorus	Algal uptake, organic mineralization, sediment flux; adsoprtion/desorption to/from particles
FRP-ADS	mmol P m^{-3}	Particulate inorganic phosphorus	Adsoprtion/desorption of/to free FRP
NH$_4^+$	mmol N m^{-3}	Ammonium	Algal uptake, nitrification, organic mineralization, sediment flux
NO$_3^-$	mmol N m^{-3}	Nitrate	Algal uptake, nitrification, denitrification, sediment flux
CPOM	mmol C m^{-3}	Coarse particulate organic matter	Breakdown to POM by macroinvertebrates
DOC-R	mmol C m^{-3}	Refractory DOC	Enzymatic hydrolysis to more labile DOM, sediment flux, photolysis
DON-R	mmol C m^{-3}	Refractory DON	
DOP-R	mmol C m^{-3}	Refractory DOP	
DOC	mmol C m^{-3}	Dissolved organic carbon	Mineralization, algal excretion
DON	mmol N m^{-3}	Dissolved organic nitrogen	
DOP	mmol P m^{-3}	Dissolved organic phosphorus	
POC	mmol C m^{-3}	Particulate organic carbon	Enzymatic hydrolysis (breakdown) to DOM, settling, algal mortality, and loss to grazing
PON	mmol N m^{-3}	Particulate organic nitrogen	
POP	mmol P m^{-3}	Particulate organic phosphorus	
TP	mmol P m^{-3}	Total Phosphorus	Sum of all P state variables
TN	mmol N m^{-3}	Total Nitrogen	Sum of all N state variables
TKN	mmol N m^{-3}	Total Kjedahl Nitrogen	Sum of relevant N state variables
CDOM	mmol C m^{-3}	Chromophoric Dissolved Organic Matter	Related from DOC-R and DOC concentrations
Plankton groups			
BAC	mmol C m^{-3}	Heterotrophic bacteria (*)	Growth based on DOM consumption, respiration and loss to grazing
SYNE	mmol C m^{-3}	*Synechoccoccus* / picoplankton (*)	Growth based on photosynthesis, respiration, excretion and mortality, and loss to grazing
BGA	mmol C m^{-3}	Cyanobacteria	
CRYPT	mmol C m^{-3}	Cryptophytes	
DIATOM	mmol C m^{-3}	Diatoms	
DINO	mmol C m^{-3}	*Karlodinium* / Dinoflagellate group	
GRN	mmol C m^{-3}	Chlorophytes	
TCHLA	ug Chla L^{-1}	Total Chlorophyll-a	Sum of the algal groups, converted to pigment concentration
ZOO$_z$	mmol C m^{-3}	Zooplankton groups (*)	Growth based on ingestion, respiration, mortality and loss to predation
Benthic groups			
MPB	mmol C m^{-2}	Microphytobenthos (*)	Growth based on photosynthesis, respiration
ZOST	mmol C m^{-2}	*Zostera* biomass (*)	
HALO	mmol C m^{-2}	*Halophila* biomass	
BIV	mmol C m^{-2}	Benthic invertebrate biomass (*)	Growth based on ingestion of filtered material, respiration, excretion and mortality
Suspended sediment and related properties			
SS$_s$	g SS m^{-3}	Suspended solids groups	Settling, resuspension
Turbidity	NTU	Turbidity	Computed based on SS, TCHLA, CPOM and POM

Geochemical variables			
DIC	mmol C m^{-3}	Dissolved inorganic carbon (*)	Photosynthesis and respiration, organic carbon mineralization, sediment flux, atmospheric flux, precipitation in carbonates
pCO$_2$	atm	Partial pressure of CO$_2$ (*)	Calculated as a function of DIC from Henry's Law
CH4	mmol C m^{-3}	Methane (*)	Produced during sediment respiration, reoxidation, sediment flux
H$_2$S	mmol S m^{-3}	Dissolved Sulfide (*)	Aqueous speciation, oxidation and reduction, sediment flux
SO$_4$	mmol SO$_4$ m^{-3}	Dissolved Sulfate (*)	
FeII	mmol Fe m^{-3}	Dissolved Ferrous Iron (*)	Aqueous speciation, oxidation and reduction, sediment flux, precipitation/dissolution of FeIII
FeIII	mmol Fe m^{-3}	Dissolved Ferric Iron (*)	
Zn	mmol Zn m^{-3}	Dissolved Zinc (*)	
Na	mmol Na m^{-3}	Dissolved Sodium (*)	
Cl	mmol Cl m^{-3}	Dissolved Chloride (*)	
Ca	mmol Ca m^{-3}	Dissolved Calcium (*)	Aqueous speciation, sediment flux
K	mmol K m^{-3}	Dissolved Potassium (*)	
Mg	mmol Mg m^{-3}	Dissolved Magnesium (*)	
Mn	mmol Mn m^{-3}	Dissolved Manganese (II) (*)	
Al	mmol Al m^{-3}	Dissolved Aluminum (*)	Aqueous speciation, precipitation/dissolution of gibbsite
pH	-	pH (*)	Computed based on charge balance at end of time-step
CHGBAL	eq	Charge Imbalance (*)	Assumes electroneutrality
Gibbsite	mmol m^{-3}	Solid phase Al(OH)$_3$ (*)	Precipitation/dissolution, settling
Fe(OH)$_3$(s)	mmol m^{-3}	Solid phase Fe(OH)$_3$ (*)	

(*) – indicates not configured in SCERM v1

BOLD – indicates a simulated state variable subject to transport and mass conservation, other variables are derived

3. Model parameterisation approach

Modelling within the AED framework

The AED Model has ability to simulate a range of physical, chemical and biological processes, that can be generally described based on:

- Water column kinetic (time-varying) chemical / biological transformations (e.g., denitrification or algal growth)
- Water column equilibrium (instantaneous) chemical transformations (e.g., PO_4 adsorption)
- Vertical sedimentation or migration
- Biogeochemical transformations in the sediment or biological changes in the benthos
- Fluxes across the air-water interface
- Fluxes across the sediment-water interface
- Fluxes across the terrestrial-water interface
- Feedback of chemical or biological attributes to physical properties of water (light extinction, drag, density)

The model is organised as a series of "modules" that can be connected. Relevant variables (Table 3) are described in the following sections, along with the science basis relevant to the Swan-Canning model setup. For the initial phase (v1) of the SCERM model, only the core variables are configured, and future proposed variables are therefore outlined in Section 4.

A Note on Notation

The remainder of this section presents the range of equations and parameterisations adopted by the various model approaches. For consistency, a standard mathematical notation is used.

N	= number of groups [integer]
a, om, z	= indices of various sub-groups of algae/phytoplankton, organic matter and zooplankton [integer]
$\chi_{C:Y}^{group}$	= the stoichiometric ratio of "group" between C and element "Y" [mmol C/mmol Y]
$f_{process}^{var}$	= function that returns the mass flux of "process" on "var" [mmol var/time]
$R_{process}^{var}$	= the rate of "process" influencing the variable "var" [/time]
F_{max}^{var}	= the maximum benthic areal flux of variable "var" [mmol var/area/time]
p_{source}^{group}	= the preference of "group" for "source" [0-1]
$\Phi_{lim}^{group}(var)$	= dimensionless limitation or scaling function to account for the effect of "lim" on "group" [-]
k^{var}	= generic fraction related to "var" [0-1]
Θ_{config}^{group}	= switch to configure selectable model component "config" for "group" [0,1,2,…]
$c, \theta, \gamma \ldots$	= coefficient [various units]

Light and Turbidity

The light climate in the SCE varies considerably over the length of the domain and throughout the year (Kostoglidis et al., 2005). In general terms, incident shortwave radiation is attenuated as it penetrates through the vertical cells of the model domain, and the attenuation of light is dependent on the specific bandwidth. For primary production, the shortwave (280-2800 nm) intensity at the surface (I_0) is partitioned to the photosynthetically active component (PAR) based on the assumption that ~45% of the incident spectrum lies between 400-700 nm (e.g., Jellison and Melack, 1993; Kirk, 1994). PAR and other light bandwidths such as ultra-violet (UV, ~3.5%) and near-infrared (NIR, ~51%), penetrate into the water column according to the Beer-Lambert Law, where K_d is a site specific parameter governing the attenuation:

$$I_i = f_i \, I_0 \exp\left(-K_{d_i} z\right) \tag{1}$$

where i refers to the specific bandwidth range (e.g., PAR, UV etc) and f_i is the fraction of light intensity within that range at the water surface. Within the SCE, Kostoglidis et al. (2005) measured K_d ranging from 0.3 to 3.5 m^{-1}, with strong variability associated with pulses of CDOM rich inflow water. CDOM was found to be the most significant factor explaining the variability in K_d, with contributions from TSS also significant when stepwise multiple regressions were performed on each site separately:

$$K_d = 0.346\,CDOM + 0.063\,TSS + 0.31 \tag{2}$$

In this study, CDOM was accurately parameterised based on a non-linear relationship with the total DOC concentration:

$$CDOM = 0.35\,e^{0.1922\,DOC} \tag{3}$$

where CDOM has units of m^{-1}, and DOC is in mg C/L. The CDOM-DOC relationship is not necessarily constant and can be variable between sites and within estuaries. TSS can be computed as the sum of inorganic material, simulated as SS, plus POC, CPOM and Chl-a. Some of the components that make up CDOM and TSS within the model vary dynamically as part of the simulations, the light extinction coefficient must therefore be broken down to account for variability in the concentrations of algal, inorganic and detrital particulates, and dissolved organic carbon levels based on specific attenuation coefficients, (K_e):

$$K_d = K_w + K_{e_s}\,SS + K_{e_d}\,(DOC + DOCR) + K_{e_p}\,(POC + CPOM) + \sum_a^{N_{PHY}}\left(K_{e_a}\,PHY_{C_a}\right) \tag{4}$$

where K_e (m^{-1} (g m^{-3})$^{-1}$) for SS and POC are assigned similar values as they were conceptually equivalent to TSS in the Kostoglidis et al. (2005) analysis. The absorption spectrum of phytoplankton varies with species, but generally peaks occur at ~430 nm and ~675 nm, with a minimum in the green region (Jeffrey, 1981), and therefore impacts upon PAR beam attenuation. Whilst K_e for Chl-a didn't come up significant for most sites in Kostoglidis et al. (2005), this was likely due to the dominance of CDOM, and experience from other estuarine sites typically report K_{e_p} as 0.01 - 0.02. Note that for the Swan model the 3rd term may be replaced by the exact CDOM computation reported above in Eq 2.

Computing turbidity from the concentration of particulates is also possible and able to be compared to routinely measured turbidity data. The relation for simulation of turbidity is able to be expressed as:

$$Turbidity = f_{t_s}\,SS + f_{t_p}\,(POC + CPOM) + \sum_a^{N_{PHY}}\left(f_{t_a}\,PHY_{C_a}\right) \tag{5}$$

where the f_{t_s} parameters are empirical coefficients, determined through site specific correlations (Table 4).

Table 4: Range of light model related parameters.

Symbol	Description	Units	Value	Comment
K_w	Background light extinction coefficient	m^{-1}	0.31, 0.325 0.32	_Swan: Kostoglidis et al. (2005) UK: Devlin et al. (2008) for SPM_
K_{e_s}	Specific light attenuation due to non-volatile SS	m^{-1} (g m^{-3})$^{-1}$	0.063 ^ 0.066 0.036 & 0.005 * 0.0259 0.08 0.094 ^	_North Sea: Los and Wijsman (2007); * small and large suspended sediments Sau Reservoir: Armengol et al. (2003) Chesapeake: Gallegos and Moore (2000); ^ coefficient is for TSS and includes POM_
K_{e_p}	Specific light attenuation due to POM	m^{-1} (g m^{-3})$^{-1}$	0.066 0.0932 0.094 ^	_UK: Devlin et al. (2008) for SPM Sau Reservoir: Armengol et al. (2003) Chesapeake: Gallegos and Moore (2000); ^ coefficient is for TSS and includes SS_
K_{e_a}	Specific light attenuation due to algae groups	m^{-1} (ug L^{-1})$^{-1}$	0.016 0.0169 0.0154	_Chesapeake: Gallegos and Moore (2000) Sau Reservoir: Armengol et al. (2003) Chesapeake: Gallegos (2001)_
K_{e_d}	Specific light attenuation due to CDOM (as DOC)	m^{-1} (g m^{-3})$^{-1}$	0.26 0.0471	_Swan: Kostoglidis et al. (2005) Fig 6 Chesapeake: Gallegos (2001)_
f_{t_s}	Coefficient between turbidity and SS	NTU (g m^{-3})$^{-1}$	0.33	_Chesapeake: Gallegos and Moore (2000) Chesapeake: Gallegos (2001) Figure 2b_
f_{t_p}	Coefficient between turbidity and POC	NTU (g m^{-3})$^{-1}$	0.825	_Chesapeake: Gallegos (2001) found POC ~40% POM (TVSS), so 0.33/0.4_
f_{t_a}	Coefficient between turbidity and algae	NTU (g m^{-3})$^{-1}$	0.825	

Oxygen

Dissolved Oxygen (DO) dynamics respond to processes of atmospheric exchange, sediment oxygen demand, microbial use during organic matter mineralisation and nitrification, photosynthetic oxygen production and respiratory oxygen consumption, chemical oxygen demand, and respiration by other biotic components such as seagrass and bivalves (Table 5).

Table 5: Mass balance and functions related to oxygen cycling.

State variable mass balance equation:

$$\frac{dO_2}{dt} = \pm f^{O_2}_{atm} - f^{O_2}_{sed} - \frac{f^{DOC}_{miner}}{\chi^{miner}_{C:O_2}} - \frac{f_{nitrif}}{\chi^{nitrif}_{N:O_2}} + \sum_a^{N_{PHY}}\left(\frac{f^{PHY_{Ca}}_{uptake}}{\chi^{PHY}_{C:O_2}}\right) - \sum_a^{N_{PHY}}\left(\frac{f^{PHY_{Ca}}_{resp}}{\chi^{PHY}_{C:O_2}}\right) - \sum_z^{N_{ZOO}}\left(\frac{f^{ZOO_z}_{resp}}{\chi^{ZOO}_{C:O_2}}\right) + \frac{\left(f^{SEA_s}_{photo} - f^{SEA_s}_{resp}\right)}{\chi^{SEA}_{C:O_2}} - \frac{f^{BIV_v}_{resp}}{\chi^{BIV}_{C:O_2}} \quad (5)$$

= ± **atmospheric O₂ exchange** (surface cells only)
- **sediment O₂ demand** (benthic cells only)
- **O₂ consumption during bacterial mineralisation of DOC**
- **O₂ consumption during nitrification**
+ **O₂ production by phytoplankton photosynthesis**
- **O₂ consumption by phytoplankton respiration**
- **O₂ consumption due to zooplankton respiration**
+ **O₂ production and consumption by seagrass due to photosynthesis and respiration** (benthic cells only)
- **O₂ consumption due to bivalve respiration** (benthic cells only)

Atmospheric exchange is typically modelled based on Wanninkhof (1992) and the flux equation of Riley and Skirrow (1974):

$$f^{O_2}_{atm} = c^{O_2}_{atm}([O_2]_{atm} - [O_2]_z) \quad (6)$$

that adopts a piston velocity, $c^{O_2}_{atm}$, that is the air-water exchange coefficient (m day^{-1}) for O₂ which is proportional to $S_c^{-1/2}$ (S_c = Schmidt Number), and varies due to windspeed and water solubility within the water (Wanninkhof, 1992):

$$S_c = (0.9 + s_H/35)[2073.1 - 125.62\,T + 3.6276\,T^2 - 0.043219\,T^3] \quad (7)$$

$$c^{O_2}_{atm} = \begin{cases} \left(\frac{0.31}{360000}\right)\frac{U_{10}^2}{\sqrt{\frac{S_c}{660}}} & Riley\ and\ Skirrow\ (1974) \\[3mm] \left(\frac{0.0283}{360000}\right)U_{10}^3 \Big/ \sqrt{S_c/660} & Wanninkhof\ and\ McGillis\ (1999) \end{cases} \quad (8)$$

The O₂ solubility (mg L^{-1} atm^{-1}) is calculated from water temperature and salinity (Weiss, 1974) as:

$$\gamma = 1.42763\,exp(B1 - B2 + B3), \quad (9)$$

where

$$B_1 = -173.4292 + 249.6339 . 100.0/(T + 273) + 143.3483 . log((T + 273)/100.0) \quad (10a)$$

$$B_2 = -21.8492 . (T + 273)/100.0 \quad (10b)$$

$$B_3 = S_H . (-0.033096 + 0.014259\ (T + 273)/100.0 - 0.0017\ ((T + 273)/100.0)^2) \quad (10c)$$

where S_H is the water salinity, T is the water temperature, U_{10} is wind speed at 10m height calculated using wind profile power law from the measured wind speed U, and $pO_{2,w}$ is the atmospheric partial pressure of O₂ (atm). Within the middle and upper reaches of the SCE much of the domain is sheltered form the prevailing wind, meaning that it is likely that the above expressions will over-estimate the exchange. For example, Valchon & Prairie (2013) identified a scaling relationship between $c^{O_2}_{atm}$ and exposed area of lakes, and a similar scaling would be appropriate for the inland regions of the SCE domain. Further work however is required to be undertaken to quantify the extent of this fetch dependence.

Modelling sediment oxygen demand can take a variety of forms. The simplest is one that varies as a function of the overlying water temperature and dissolved oxygen levels:

$$f_{sed}^{O_2} = F_{max}^{O_2} \frac{O_2}{K_{sed}^{O_2} + O_2} \left(\theta_{sed}^{O_2}\right)^{T-20} \tag{11}$$

The above oxygen model is reasonably simple and found to work well in the Upper Swan by Hipsey et al. (2013), and similarly Bruce et al. (2014) used an identical model with good success in the Yarra River estuary. However, other more dynamic options are available and discussed in more detail in the Sediment section.

Other processes impacting the oxygen concentration include the breakdown of DOC by aerobic heterotrophic bacteria to CO_2, whereby a stoichiometrically equivalent amount of oxygen is removed. Chemical oxidation, for example processes such as nitrification or sulfide oxidation, also consume oxygen dependent on the relevant stoichiometric factor. Photosynthetic oxygen production and respiratory oxygen consumption by pelagic phytoplankton is also included and is summed over the number of simulated phytoplankton groups. Seagrass interaction with the oxygen cycle is configurable within the model, however for the SCE implementation v1, the seagrass biomass is included without feedbacks to the biogeochemical cycles.

Organic matter and nutrients

Several studies have previously described nutrient and organic matter dynamics within the SCE and patterns of nutrient loading to the system (Hamilton et al., 2006; Robson et al., 2008; Petrone et al., 2009; Petrone, 2010; Fellman et al., 2011). Of importance are the dissolved inorganic fractions, FRP, NO_x and NH_4, and the various organic matter (OM) pools. Both the inorganic and organic, and dissolved and particulate forms of C, N and P are therefore modelled explicitly along the general degradation pathway of POM to DOM to dissolved inorganic matter (DIM), however the need for discrete OM pools is elaborated upon below. The nitrogen cycle includes the additional processes of denitrification, nitrification and N_2 fixation (discussed in the phytoplankton section), that are not in the carbon and phosphorus cycles, though note N_2 levels are not tracked as a state variable. The silica cycle is also represented but is more straightforward and needs to simply include the processes of biological uptake of dissolved Si (RSi) by diatoms into the internal Si (ISi) pool, dissolved sediment fluxes of RSi, diatom mortality directly into the RSi sediment pool, settling of ISi. This relatively simple representation assumes that diatom frustules rapidly mineralize.

Within the SCE, it is well established that both autochthonous and allochthonous sources of OM have important consequences for water quality. Reactivity of OM is known to be linked with origin, varying potentially orders of magnitude, and including a single OM pool for a site like the SCE is likely to be a significant over-simplification. Harvey and Mannio (2001) analysed samples from several points in a US estuary according to an uncharacterisable fraction and a few major molecular classes (carbohydrates, proteins, lipids, lignins and hydrocarbons), and identified significant changes along the estuarine gradient. Although using a simpler analytical method, Fellman et al. (2011) similarly identified within the SCE a transition in the nature of the DON molecular fractions from the freshwater source to the ocean with implications for the reactivity of DOM along the gradient of the estuary. As identified by Petrone et al. (2009) and Petrone et al. (2011), the DOC reactivity can be variable but is largely refractory, and less reactive than DON. Within the particulate pool, similarly there is a relatively labile POM fraction based on internal generation, and inputs from urban drains, in addition to a more refractory coarse POM pool (CPOM) that originates mainly form the forested headwaters and regions with significant intact riparian vegetation.

An 8-pool organic matter module is therefore required, as outlined in Figure 2, able to capture the variable reactivity of the OM pool and its stoichiometry. For parameterization of this model, only limited data is available, including for both the stoichiometry, breakdown and tributary input so the different fractions must be assumed. Analysis by Petrone et al. (2009) identify that the reactive fraction of DOC in inflowing water was ~10%, whereas for DON it was closer to 30%. Based on analysis of available TOC and DOC data from the estuary the POC fraction can be estimated as being only 10% of TOC (R^2 = 0.92). Unfortunately, there is limited information on the composition or amount of CPOM, however, it is thought to be a significant under certain flow conditions. Refer to Table 10 for a list of relevant parameters and estimates of values.

Internally generated inputs of POM also include shedding of seagrass leaves (this happens en-mass usually associated with winds/storms) and also decomposition of macroalgae (again a seasonality with decomposition occurring prob mid-summer). These latter terms are not presently included but reserved for future development efforts.

Under this conceptual model the decomposition of particulate detrital material is broken down through a process of enzymatic hydrolysis that slowly converts POM to labile DOM. A small fraction, f_{ref}, of this material is diverted to the DOM-R pool. The bioavailable DOM material enters the bacterial terminal metabolism pathways. These are active depending on the ambient oxygen concentrations and presence of electron acceptors, and of most relevance to the SCE, these pathways aerobic breakdown, denitrification, sulfate reduction, and methanogenesis. In most model approaches it is assumed these communities vary in response to temperature, and are mediated using a simple oxygen dependence or limitation factor. Ultimately, extending the mineralization rates to be computed from thermodynamic arguments is possible and has been discussed recently by Paraska et al. (2014), with the potential for advances in this area as analytical tools for NOM characterization are applied within the SCE system. Reoxidation of reduced by-products is also included to account the role of nitrifiers, sulfate oxidising bacteria (SOB) and methane oxidising bacteria (MOB).
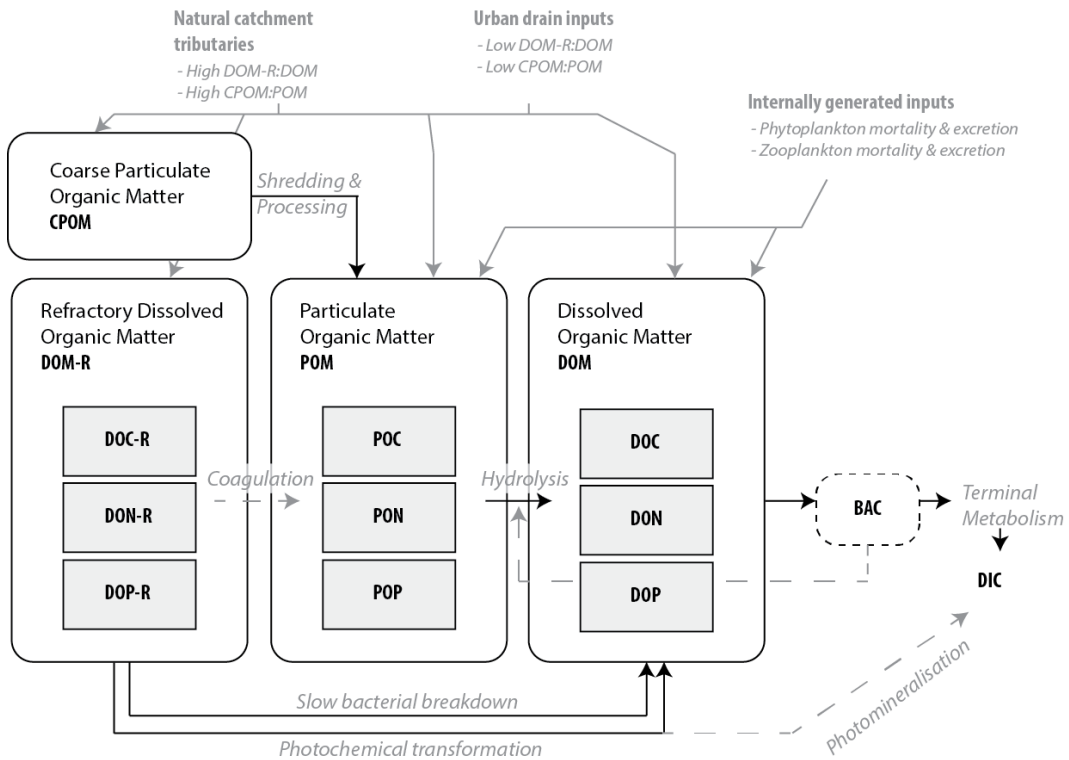

Figure 2. Schematic overview of organic matter (OM) pools and their interactions. Grey dashed line indicates optional process pathway. Different tributaries to the model must be prescribed OM pool boundary concentrations based on land-use specific ratios of POM and DOM reactivity.

Ultraviolet light is also known to drive photochemical breakdown of chromophoric DOM, conceptually equivalent to the DOM-R pool in Figure 2. This photolysis process can take shape either as phototransformation of complex DOM-R molecules to more bioavailable molecules (ie., DOM in Figure 2), or as photomineralisation, where by components of the DOM-R molecule are mineralised. This is modelled based on a known intensity of UV photons, which drives a stoichiometrically equivalent loss of DOM-R via the photolysis reaction, and f_{photo} is introduced as an empirically defined fraction that indicates the extent to which the process transforms the DOM-R molecules to bioavailable molecules or completely mineralises them. The rate of photolysis can be computed based on the apparent quantum yield, ϕ_λ, which varies with wavelength, the scalar photon flux density, $\hat{I}_\lambda$, and the adsorption coefficient, α_λ, by integrating across the active wavelength spectrum, λ_{max} to λ_{min}. This can be approximated for b discrete bandwidths (e.g. UV-A, UV-B, PAR) to simplify the calculation as:

$$R_{pm}^{DOM-R} = \int_{\lambda_{min}}^{\lambda_{max}} \phi_\lambda \hat{I}_\lambda \alpha_\lambda \, d\lambda \approx \sum_{b=1}^{3} \bar{\phi}_b \hat{I}_b \alpha_b \qquad (12)$$

where $\hat{I}_b$ is the mean bandwidth intensity (mol photons m^{-2} s^{-1}) computed from the light intensity at any given depth, I, $\bar{\phi}_b$ is the mean bandwidth quantum yield, and α_b is the mean absorbance across the window of the specific bandwidth being computed. The latter two can be approximated by substituting into the following (Vähätalo et al. 2000; Vähätalo and Zepp, 2005): $\phi_\lambda = c\ 10^{-d\lambda}$ and $\alpha_\lambda = \alpha_x \exp\left(-S[x - \lambda]\right)$.

Filterable reactive phosphorus also is known to adsorb onto suspended solids (SS), however, the rate is often site specific (Froelich, 1988). In particular the adsorbed fraction varies considerably within estuaries depending on the nature of the particle origin and their size distribution, and both Langmuir and Freundlich isotherm models have been demonstrated to capture the adsorption process well (Zhang et al., 2009). Adsorption also varies considerably along a salinity gradient (Sundareshwar and Morris, 1999). For this process adoption of the Langmuir isotherm model, as implemented by Chao et al. (2010), is a convenient method, but modified to account for pH and salinity (see equation in Table 8). However, there is limited local information of PO_4 adsorption by which to set the parameters. Both CO_2 and CH_4 are also assumed to flux across the air-water interface, adopting a similar transfer approach as described for oxygen.

The above description is summarized in the below tables (Table 6-9) in the form of balance equations. These are written in generic form according to the standard notation described earlier, and assuming the generic parameterizations as listed below. Table 10 summarises the parameters used within these parameterizations.

Generic process parameterisations:

$$f_{sett}^{VAR} = \frac{\omega_{VAR}}{dz_z}[VAR] \qquad \text{sedimentation of particulate material} \qquad (13)$$

$$f_{decom}^{VAR} = R_{decom}^{VAR}\frac{[O_2]}{K_{decom}+[O_2]}\left(\theta_{decom}\right)^{T-20}[VAR] \qquad \text{hydrolysis/decomposition/breakdown of POM or CPOM} \qquad (14)$$

$$f_{miner}^{VAR} = R_{miner}^{VAR}\frac{[O_2]}{K_{miner}+[O_2]}\left(\theta_{miner}\right)^{T-20}[VAR] \qquad \text{aerobic mineralisation of labile (non-chromophoric) DOM} \qquad (15)$$

$$+ f_{denit}^{NO_3}\chi_{denit}^{VAR} \qquad \text{anaerobic mineralisation of labile DOM by denitirification} \qquad (16)$$

$$f_{denit}^{NO_3} = R_{denit}\frac{K_{denit}}{K_{denit}+[O_2]}\left(\theta_{denit}\right)^{T-20}[NO_3] \qquad \text{denitrification rate} \qquad (17)$$

$$f_{nitrif}^{NH_4} = R_{nitrif}\frac{[O_2]}{K_{nitrif}+[O_2]}\left(\theta_{nitrif}\right)^{T-20}[NH_4] \qquad \text{nitrification rate} \qquad (18)$$

$$f_{atm}^{VAR} = \begin{cases} \frac{c_{atm}^{VAR}([VAR]_{atm}-[VAR]_z)}{dz_s} & if\ z = z_s \\ 0 & if\ z \neq z_s \end{cases} \qquad \text{atmospheric flux} \qquad (19$$

$$f_{photo}^{VAR} = R_{pm}^{VAR}[VAR] \qquad \text{photochemical breakdown flux} \qquad (20)$$

$$f_{sed}^{VAR} = F_{max}^{VAR}\frac{K_{sed}^{VAR}}{K_{sed}^{VAR}+[DO]}\left(\theta_{sed}^{VAR}\right)^{T-20}\left(\frac{\widehat{A_z}}{dz_z}\right) \qquad \text{sediment flux} \qquad (21)$$

where $\widehat{A_z} = A_z^{ben}/A_z$ is the fraction of the cell in contact with the sediment and dz_z is the thickness of the zth layer/cell.

Table 6: Mass balance and functions related to <u>silica</u> cycling.

State variable mass balance equations:

$$\frac{dRSi}{dt} = +f_{sed}^{RSi} - \sum_a^{N_{PHY}} f_{uptake}^{PHY-Si_a} + \sum_a^{N_{PHY}} f_{excr}^{PHY-Si_a} \qquad (22)$$

$= \pm$ **sediment flux**
   – **uptake by phytoplankton groups**
   – **excretion by phytoplankton groups**

PHY_{Si} is also included in the Si cycle and described in the phytoplankton module

Table 7: Mass balance and functions related to <u>carbon</u> cycling.

State variable mass balance equations:

$$\frac{dCH_4}{dt} = \pm f_{atm}^{CH_4} - f_{ox}^{CH_4} + f_{sed}^{CH_4} \tag{23}$$

  = ± atmospheric CH₄ exchange
    – oxidation to DIC by methane oxidizing bacteria (MOB)
    + sediment flux

$$\frac{dDIC}{dt} = \pm f_{atm}^{CO_2} + f_{miner}^{DOC} + f_{photo} f_{photo}^{DOCR} + f_{ox}^{CH_4} \pm f_{sed}^{DIC} + \sum_{a}^{N_{PHY}} \left[f_{resp}^{PHY_{Ca}} - f_{uptake}^{PHY_{Ca}} \right] + \sum_{z}^{N_{ZOO}} f_{resp}^{z} \tag{24}$$

  = ± atmospheric CO₂ exchange
    + respiration by bacteria during DOM breakdown
    + photomineralisation of chromophoric DOM (DOC-R)
    + oxidation to DIC
    ± sediment flux
    ± carbon fixation and respiration by phytoplankton groups
    + respiration by zooplankton groups

$$\frac{dDOC}{dt} = (1 - f_{ref}) f_{decom}^{POC} + (1 - f_{photo}) f_{photo}^{DOCR} - f_{miner}^{DOC} \pm f_{sed}^{DOC} + \sum_{a}^{N_{PHY}} f_{excr}^{PHY\_C_a} + \sum_{z}^{N_{ZOO}} f_{excr}^{z} \tag{25}$$

  = + decomposition from particulate detritus (POC)
    + phototransformation of chromophoric DOM (DOC-R)
    – mineralisation by bacteria
    ± sediment flux
    – excretion by phytoplankton groups
    – excretion by zooplankton groups

$$\frac{dDOC\_R}{dt} = f_{ref} f_{decom}^{POC} - f_{miner}^{DOCR} - f_{photo}^{DOCR} \pm f_{sed}^{DOCR} \tag{26}$$

  = + accumulation during particulate detritus (POC) mineralisation
    – slow mineralisation by bacteria
    – photolysis of chromophoric DOM (DOC-R)
    ± sediment flux

$$\frac{dPOC}{dt} = f_{bdown}^{CPOM} - f_{decom}^{POC} - f_{sett}^{POC} + \sum_{a}^{N_{PHY}} f_{mort}^{PHY\_C_i} + \sum_{z}^{N_{ZOO}} \left[(1 - k_{assim}^{z}) f_{assim}^{z} + (1 - k_{fsed}^{z}) f_{fecal}^{z} + f_{mort}^{z} \right] \tag{27}$$

  = + breakdown of CPOM
    – decomposition to DOC
    ± sedimentation
    + mortality from phytoplankton groups
    + messy feeding, faecal pellet release and mortality from zooplankton groups

$$\frac{dCPOM}{dt} = -f_{bdown}^{CPOM} - f_{sett}^{CPOM} \tag{28}$$

  = – breakdown of CPOM
    ± sedimentation

Balance equations for PHY_C and ZOO_C are described in the phytoplankton and zooplankton sub-sections below.

Total Organic Carbon

$$TOC = DOC + DOC\_R + POC + \sum_{a}^{N_{PHY}} PHY_{C_a} + \sum_{z}^{N_{ZOO}} ZOO_z \tag{29}$$

State variable mass balance equations:

$$\frac{dNH_4}{dt} = f_{miner}^{DON} + f_{photo}\, f_{photo}^{DONR} - f_{nitrif}^{NH_4} + f_{sed}^{NH_4} - \sum_{a}^{N_{PHY}} \left[p_{NH_4}^{a} \times f_{uptake}^{PHY\_N_a} \right] \tag{30}$$

   = + mineralization from DON
    + photomineralisation of chromophoric DOM (DON-R)
    – nitrification
    ± sediment flux
    – uptake from the phytoplankton community

$$\frac{dNO_3}{dt} = +f_{nitrif}^{NH_4} - f_{denit}^{NO_3} - f_{sed}^{NO_3} - \sum_{a}^{N_{PHY}} \left[p_{NO_3}^{a} \times f_{uptake}^{PHY\_N_a} \right] \tag{31}$$

   = + nitrification
    – denitrification
    ± sediment flux
    – uptake from the phytoplankton community

$$\frac{dDON}{dt} = (1 - f_{ref})f_{decom}^{PON} + (1 - f_{photo})f_{photo}^{DONR} - f_{miner}^{DON} + f_{sed}^{DON} + \sum_{a}^{N_{PHY}} f_{excr}^{PHY\_N_a} + \sum_{z}^{N_{ZOO}} \frac{f_{excr}^{z}}{\chi_{C:N}^{z}} \tag{32}$$

   = + decomposition from particulate detritus (PON)
    + phototransformation of chromophoric DOM (DON-R)
    – mineralisation by bacteria
    ± sediment flux
    – excretion by phytoplankton groups
    – excretion by zooplankton groups

$$\frac{dDON\_R}{dt} = f_{ref}f_{decom}^{PON} - f_{miner}^{DONR} - f_{photo}^{DONR} \pm f_{sed}^{DONR} \tag{33}$$

   = + accumulation during particulate detritus (POM) mineralisation
    – slow mineralisation by bacteria
    – photolysis of chromophoric DOM (DON-R)
    ± sediment flux

$$\frac{dPON}{dt}$$

$$= f_{bdown}^{CPOM}\, \chi_{C:N}^{CPOM} - f_{decom}^{PON} - f_{sett}^{PON} + \sum_{i}^{N_{PHY}} f_{mort}^{PHY\_N_a} + \sum_{z}^{N_{ZOO}} \left[(1 - k_{assim}^{z})f_{assim}^{z} + (1 - k_{fsed}^{z})f_{fecal}^{z} + f_{mort}^{z} \right] \frac{1}{\chi_{C:N}^{z}} \tag{34}$$

   = + breakdown of CPOM
    – decomposition to DON
    ± sedimentation
    + mortality from phytoplankton groups
    + messy feeding, faecal pellet release and mortality from zooplankton groups

Balance equations for PHY_N and ZOO_N are described in the phytoplankton and zooplankton sub-sections below.

Total Nitrogen

$$TN = NO3 + NH4 + DON + DON\_R + PON + \sum_{a}^{N_{PHY}} PHY_{N_a} + \sum_{z}^{N_{ZOO}} \frac{ZOO_z}{\chi_{C:N}^{z}} \tag{35}$$

Total Kjeldahl Nitrogen

$$TKN = NH4 + DON + DON\_R + PON + \sum_{a}^{N_{PHY}} PHY_{N_a} + \sum_{z}^{N_{ZOO}} \frac{ZOO_z}{\chi_{C:N}^{z}} \tag{36}$$

Table 9: Mass balance and functions related to <u>phosphorus</u> cycling.

State variable mass balance equations:

$$\frac{dPO_4}{dt} = f_{miner}^{DOP} + f_{photo} f_{photo}^{DOPR} + f_{sed}^{PO_4} \pm f_{ads}^{PO_4} - \sum_{a}^{N_{PHY}} \left[f_{uptake}^{PHY\_P_a} \right]$$
(37)

  = + mineralization from DOP
    + photomineralisation of chromophoric DOM (DOP-R)
    ± sediment flux
    ± **adsorption/desorption** (assigned to satisfy equilibrium equation below)
    – uptake from the phytoplankton community

$$\frac{dPO_4^{ads}}{dt} = \pm f_{ads}^{PO_4} - f_{sett}^{PO_4^{ads}}$$
(38)

  = ± **adsorption/desorption** (assigned to satisfy equilibrium equation below)
    ± **sedimentation**

$$\frac{dDOP}{dt} = (1 - f_{ref}) f_{decom}^{POP} + (1 - f_{photo}) f_{photo}^{DOPR} - f_{miner}^{DOP} + f_{sed}^{DOP} + \sum_{a}^{N_{PHY}} f_{excr}^{PHY\_P_a} + \sum_{z}^{N_{ZOO}} 1/\chi_{C:P}^z f_{excr}^z$$
(39)

  = + **decomposition** from particulate detritus (POP)
    + **phototransformation** of chromophoric DOM (DOP-R)
    – **mineralisation** by bacteria
    ± sediment flux
    – excretion by phytoplankton groups
    – excretion by zooplankton groups

$$\frac{dDOP\_R}{dt} = f_{ref} f_{decom}^{POP} - f_{miner}^{DOP} - f_{photo}^{DOPR} + f_{sed}^{DOP} + \sum_{a}^{N_{PHY}} f_{excr}^{PHY\_P_a} + \sum_{z}^{N_{ZOO}} 1/\chi_{C:P}^z f_{excr}^z$$
(40)

  = + **decomposition** from particulate detritus (POP)
    – **mineralisation** by bacteria
    – **photolysis** of chromophoric DOM (DOP-R)
    ± sediment flux
    – excretion by phytoplankton groups
    – excretion by zooplankton groups

$$\frac{dPOP}{dt} = f_{bdown}^{CPOM} \chi_{C:P}^{CPOM} - f_{decom}^{POP} - f_{sett}^{POP} + \sum_{a}^{N_{PHY}} f_{mort}^{PHY\_P_a} + \sum_{z}^{N_{ZOO}} \left[(1 - k_{assim}^z) f_{assim}^z + (1 - k_{fsed}^z) f_{fecal}^z + f_{mort}^z \right] \frac{1}{\chi_{C:P}^z}$$

  = + **breakdown** of CPOM
    – **decomposition** to DOP
(41)
    ± **sedimentation**
    + mortality from phytoplankton groups
    + messy feeding, faecal pellet release and mortality from zooplankton groups

Balance equations for PHY_P and ZOO_P are described in the phytoplankton and zooplankton sub-sections below.

Total Phosphorus

$$TP = PO_4 + PO_4^{ads} + DOP + DOP\_R + POP + \sum_{a}^{N_{PHY}} PHY_{P_a} + \sum_{z}^{N_{ZOO}} \frac{ZOO_z}{\chi_{C:P}^z}$$
(42)

Total Inorganic Phosphate
$$TPO_4 = PO_4 + PO_4^{ads}$$
(43)

Adsorbed PO4 fraction at equilibrium
(44)

$$PO_4^{ads} = \frac{1}{2TPO_4} \left[\left(TPO_4 + \frac{1}{c_{ads}^r} + c_{ads}^{max} \Phi_{ads}^{pH}(pH) SS \right) - \sqrt{ \left(TPO_4 + \frac{1}{c_{ads}^r} + c_{ads}^{max} \Phi_{ads}^{pH}(pH) SS \right)^2 + \frac{4 c_{ads}^{max} \Phi_{ads}^{pH}(pH)}{c_{ads}^r} SS } \right]$$

Table 10: Summary of water column biogeochemical parameter descriptions, units and typical values.

Symbol	Description	Units	Value	Comment
	Atmospheric exchange			
$k_{atm}^{O_2}$	oxygen transfer coefficient	m s^{-1}		calculated *Wanninkhof (1992)*
$[O_2]_{atm}$	atmospheric oxygen concentration	mmol O$_2$ m^{-3}		calculated *Riley and Skirrow (1975)*
$k_{atm}^{CO_2}$	carbon dioxide transfer coefficient	m s^{-1}		calculated
$[CO_2]_{atm}$	atmospheric carbon dioxide concentration	mmol C m^{-3}		calculated
$k_{atm}^{CH_4}$	methane transfer coefficient	m/s		calculated
$[CH_4]_{atm}$	atmospheric methane concentration	mmol C m^{-3}		calculated
$dz_{s_{min}}$	Minimum depth of a surface cell for flux computation	m	0.2	*Chosen to prevent large concentrations*
	Chemical oxidation			
$\chi_{N:O_2}^{nitrif}$	stoichiometry of O$_2$ consumed during nitrification	g N g O$_2^{-1}$	0.44	*14/32*
R_{nitrif}	maximum rate of nitrification	d^{-1}	0.5	0.5 [B]
K_{nitrif}	half saturation constant for oxygen dependence of nitrification rate	mmol O$_2$ m^{-3}	78.1	78.1 [B]
θ_{nitrif}	temperature multiplier for nitrification	-	1.08	1.08 [B]
$\chi_{CH_4:O_2}^{nitrif}$	stoichiometry of O$_2$ consumed during CH$_4$ oxidation	g C g O$_2^{-1}$	0.38	*12/32*
R_{ch4ox}	maximum rate of methane oxidation	d^{-1}	0.5	0.5 [B]
K_{ch4ox}	half saturation constant for oxygen dependence of methane oxidation rate	mmol O$_2$ m^{-3}	78.1	78.1 [B]
θ_{ch4ox}	temperature multiplier for methane oxidation	-	1.08	1.08 [B]
	Dissolved organic matter transformations			
$\chi_{C:O_2}^{miner}, \chi_{C:O_2}^{PHY}$	stoichiometry of O$_2$ consumed during aerobic mineralization and photosynthesis	g C g O$_2^{-1}$	0.38	*12/32*
$R_{miner}^{DOC}, R_{miner}^{DON}, R_{miner}^{DOP}$	maximum rate of aerobic mineralisation of labile dissolved organic matter @ 20C	d^{-1}	0.5	0.001 – 0.006 [D] 0.01 – 0.05 [A] 0.001 – 0.028 [D]
$K_{miner}^{DOC}, K_{miner}^{PON}, K_{miner}^{DOP}$	half saturation constant for oxygen dependence on aerobic mineralisation rate	mmol O$_2$ m^{-1}	31.25	47 – 78 [A]
$\theta_{miner}^{DOC}, \theta_{miner}^{DON}, \theta_{miner}^{DOP}$	temperature multiplier for aerobic mineralisation	-	1.08	1.05 – 1.11
R_{denit}	maximum rate of denitrification	d^{-1}	0.5	0.5 [B]
K_{denit}	half saturation constant for oxygen dependence of denitrification	mmol O$_2$ m^{-3}	21.8	21.8 [B]
θ_{denit}	temperature multiplier for temperature dependence of denitrification	-	1.08	1.08 [B]
R_{photo}^{DOCR}	maximum rate DOM-R photolysis per mol of light	mmol C m^{-3} d^{-1}		calculated from Eq 12 using c = 7.52 and d = 0.0122, assuming 3 bandwidth fractions based on mean wavelengths of 298, 358 and 440 nm
f_{photo}	fraction of DOM-R photolysis that leads to mineralisation	-	0.1	assumed
	Particulate organic matter transformations			
$R_{decom}^{POC}, R_{decom}^{PON}, R_{decom}^{POP}$	maximum rate of decomposition of particulate organic material @ 20C	d^{-1}	0.5	0.01 – 0.07 [A]; 0.008 [C]
$K_{decom}^{DOC}, K_{decom}^{PON}, K_{decom}^{DOP}$	half saturation constant for oxygen dependence on particulate decomposition (hydrolysis) rate	mmol O$_2$ m^{-3}	31.25	47 – 78 [A]
$\theta_{decom}^{POC}, \theta_{decom}^{PON}, \theta_{decom}^{POP}$	temperature multiplier for temperature dependence of mineralisation rate	-	1.08	1.08 [B]
R_{bdown}^{CPOM}	Rate of breakdown of CPOM to POM	d^{-1}	0.0003	10% per year
$\chi_{C:N}^{CPOM}, \chi_{C:P}^{CPOM}$	C:N and C:P stoichiometry of CPOM	mol:mol	106:16:1	Redfield
$\omega_{POC}, \omega_{PON}, \omega_{POP}$	settling rate of particulate organic material	m d^{-1}	-0.05	-1.0 [B]
ω_{CPOM}	settling rate of coarse particulate organic material	m d^{-1}	-0.1	assumed
f_{ref}	Fraction of POM breakdown that returns to DOM-R	-	0.01	assumed
	Adsorption/desorption parameters			
$\Phi_{ads}^{pH}(pH)$	Function characterizing pH effect on	-	calculated	-0.0088(pH)^2 + 0.0347(pH) + 0.9768 [E]
c_{ads}^r	ratio of adsorption and desorption rate coefficients	L mg^{-1}	0.7	0.7 [F]
c_{ads}^{max}	maximum adsorption capacity of SS	mmol P mg SS^{-1}	0.00016	0.00016 [F]

Parameters based on the following information:

[A]   Converted from data on oligotrophic lakes (Romero *et al.*, 2004) to eutrophic lakes (Gal *et al.*, 2009), and justifications therein.

[B]   Based on Bruce et al. (*2011*) FABM-AED application on the Yarra Estuary (Victoria); estimated from data from Roberts *et al.* (2013).

[C]   Based on Hamilton and Schladow (1997) for Prospect Reservoir

[D]   Based on incubations by Petrone *et al.* (2009) for Swan Estuary (Western Australia)

[E]   Based on regression of data from Salmon *et al.* (subm) based on data review from 6 papers therein

[F]   Based on model of Chao *et al.* (2010).

Sediment oxygen and nutrient fluxes

Several reported attempts have been made to measure sediment oxygen demand and nutrient fluxes within the SCE (see Table 11), however these are not easily transferable to a 3D model due to highly variable conditions under which they were measured. As highlighted in the above oxygen and nutrient sub-sections, one of the key drivers of estuarine water quality is the sediment biogeochemical processes (Crowe et al., 2012). The above sections introduced the "static" sediment flux algorithm that is suited to short-term studies where the OM concentration is thought to be relatively stable. Typical parameters for such a simple sediment model for the SCE are summarised in Table 12.

Recently the model by Zhu et al., (2016) of the Gippsland Lakes adopted a single compartment sediment model to predict the oxygen drawdown rate at the sediment-water interface accounting for a linear decay of organic matter following deposition. A more sophisticated two layer model has recently been reported for Chesapeake Bay (Testa et al., 2013). Norlem et al. (2013), undertook a full multi-layered sediment diagenesis modeling study of the Upper Swan and compared predictions against porewater data from Geoscience Australia (Smith et al., 2010). This complex model was run with steady and unsteady water column boundary conditions and found to approximate the simple Monod approach summarized above with relative accuracy under conditions of high sediment organic matter concentrations (Figure 3). Ultimately, closure of the nutrient and mass balances requires a detailed treatment of sediment organic matter process (and oxygen consumption), which creates new challenges both due to computational demand and also due to data limitations.

Table 11: Prior sediment related studies.

| Measurement	Location	Varibales	Period	Reference	
Sediment surface grabs samples	KMO WMP VIT RPB	NH_4^+ NO_X N_2 PO_4^{3-} SiO_4^{4-} DIC	May 2008	Smith et al. (2010)	Geoscience Australia Report
		DIC TOC – gives R_{OM}	12 – 24 h incubation		
	RON RCE BRW10 KIN KMO VIT SUC BBO MEA MUL WMP-RB SCS01 CAV REG MBS MSB JBC POL	NH_4^+ NO_X N_2 PO_4^{3-} SiO_4^{4-} DIC	September 2007		
		DIC TOC – gives R_{OM}	12 – 24 h incubation		
Cores	KMO WMP VIT RPB	NH_4^+ NO_X N_2 PO_4^{3-} SiO_4^{4-}	May 2008	Smith et al. (2010)	Geoscience Australia Report
	KMO WMP	NH_4^+ NO_X N_2 PO_4^{3-} SiO_4^{4-} DIC O_2TN TP			
	SR32 SR33 SR34	NH_4^+ NO_x PO_4^{3-} SiO_4^{4-} TCO_2 DON	October 2006	Smith et al. 2006	Geoscience Australia Report
	SR33	Al As Cd Cu Fe Mn Ni V Zn			
Benthic fluxes	SR32 SR1 KMO WMP	NH_4^+ NO_X N_2 PO_4^{3-} SiO_4^{4-} DIC O_2	October 2006 May 2008	Smith et al. (2010)	Geoscience Australia Report
	SR33	Al As Cd Cu Fe Mn Ni V Zn	October 2006	Smith et al. (2006)	Geoscience Australia Report
	Pelican Pt Melville Water Lucky Bay Perth Water Garrat Rd Br Ron Courtney Island Guildford	SOD NH_4^+ NO_3^- DIN FRP	February 1997	Lavery et al. (2001)	Journal paper
	Kent St Weir	SRP before and after application of Phoslock	February 2010	Application of Phoslock™ to the Canning River 2010 – Report on methods and results	DoW Report
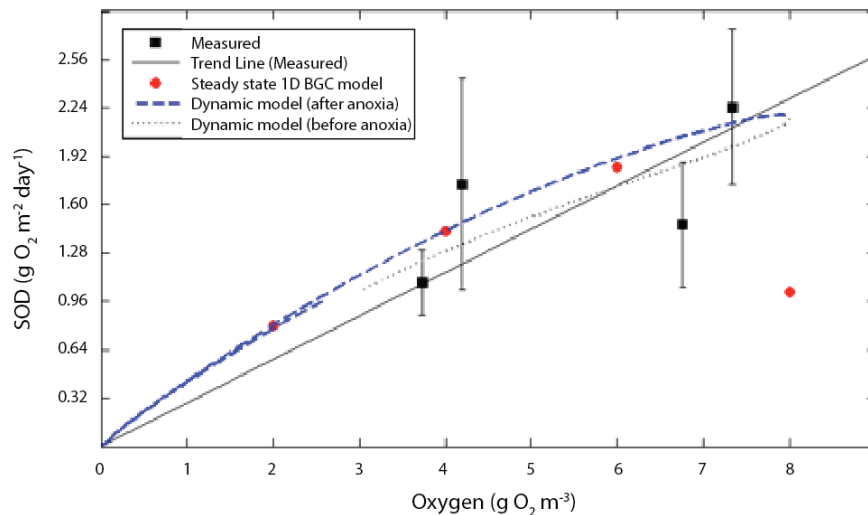
Figure 3: Sediment oxygen demand predictions from the 1D sediment diagenesis model of Norlem et al. (2013) under different bottom water oxygen conditions. Measured values are given as average +/- one standard deviation and based on data presented in Smith et al. (2010). Model simulations were run in steady state for a given bottom water condition, and also under dynamic oxygenation scenarios with variable bottom water concentrations. The latter accounts for hysteresis and delayed effects due to oxygen penetration and reaction rates.

Transitioning to a dynamic sediment diagenesis model within the SCE model system requires integration of one of the above options with the water column biogeochemistry. Currently a sediment digenesis model has been implemented within the FABM-AED framework, similar to the Norlem et al. (2013) study, and this may be applied (Figure 4); the BROM model is also now available within FABM (Yakushev et al., 2016). This does require specification of "zones" of relatively homogenous sediment attributes (e.g. particle sizes and TOC fractions). This will facilitate the development of dynamic predictions of nutrient release, for example, recycling of material following an algal bloom, or after deposition from a flood pulse. This approach is also ultimately necessary if we are to compute the persistence of OM in the sediment and understand the long-term trajectory of estuary water quality over decadal scales. Parameterisation of the effect of benthic macroinvertebrates depending on environmental conditions such as oxygen concentration is also an important process that needs further development.
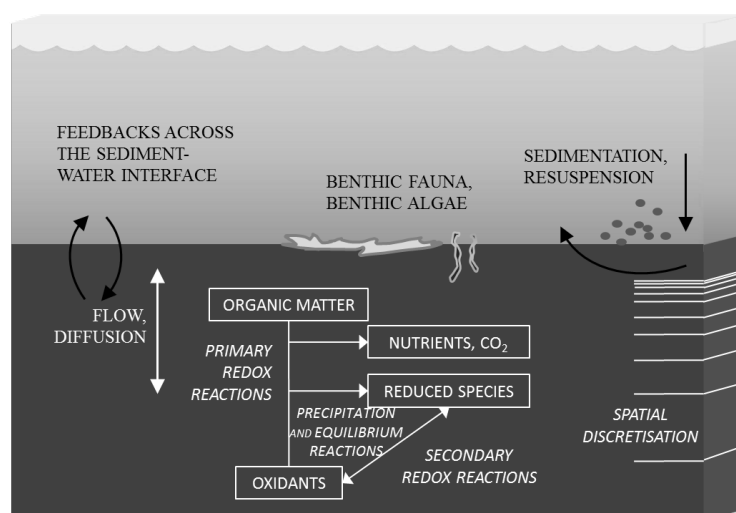

Figure 4: Overview of sediment diagenesis model, indicating physical and chemical processes impacting sediment quality (taken from Paraska et al., 2014).

Table 12: Summary of sediment parameter descriptions, units and typical values.

Symbol	Description	Units	Assigned value	Comment
$F_{max}^{O_2}$	maximum flux of oxygen across the sediment water interface into the sediment	mmol O_2 m^{-2} d^{-1}	80.0	*Lake:* 22.4 [G] *River:* 9.4 – 20.3 [B] *Estuary:* 48 [C]; 79 [D]; ~50 [E]
$K_{sed}^{O_2}$	half saturation constant for oxygen dependence of sediment oxygen flux	mmol O_2 m^{-3}	130	*Estuary:* 150 [C]; ~50 [F]
$\theta_{sed}^{O_2}$	temperature multiplier for temperature dependence of sediment oxygen flux	-	$= \theta_{sed}$ =1.08	1.04 – 1.10 [A]
F_{max}^{RSi}	maximum flux of silica across the sediment water interface	mmol Si m^{-2} d^{-1}	4	*Estuary:* 4 – 40 [E]
K_{sed}^{RSi}	half saturation constant for oxygen dependence of sediment silica flux	mmol Si m^{-3}	150	estimated
θ_{sed}^{RSi}	temperature multiplier for temperature dependence of sediment silica flux	-	$= \theta_{sed}$ =1.08	1.04 – 1.10 [A]
$F_{max}^{PO_4}$	maximum flux of phosphate across the sediment water interface	mmol P m^{-2} d^{-1}	0.2	*Lake:* 0.01 – 0.07 [G] *River:* 0.01 – 0.10 [B] *Estuary:* 0.3 – 4 [E]
$K_{sed}^{PO_4}$	half saturation constant for oxygen dependence of sediment phosphate flux	mmol O_2 m^{-3}	20	*Estuary:* >200 [F]
$\theta_{sed}^{PO_4}$	temperature multiplier for temperature dependence of sediment phosphate flux	-	$= \theta_{sed}$ =1.08	1.04 – 1.10 [A]
F_{max}^{DOP}	maximum flux of dissolved organic phosphorus across the sediment water interface	mmol P m^{-2} d^{-1}	0.05	*River:* 0.05 – 0.10 [B]
K_{sed}^{DOP}	half saturation constant for oxygen dependence of sediment dissolved organic phosphorus flux	mmol O_2 m^{-3}	150	estimated
θ_{sed}^{DOP}	temperature multiplier for temperature dependence of sediment dissolved organic phosphorus flux	-	$= \theta_{sed}$ =1.08	1.04 – 1.10 [A]
$F_{max}^{NH_4}$	maximum flux of ammonium across the sediment water interface	mmol N m^2 d^{-1}	30.0	*Lake:* 1.3 [G] *River:* 4.3 – 12.8 [B] *Estuary:* 30 [C]; 5 – 25 [E]
$K_{sed}^{NH_4}$	half saturation constant for oxygen dependence of sediment ammonium flux	mmol N m^{-1}	31.25	*Estuary:* 31.25 [C]
$\theta_{sed}^{NH_4}$	temperature multiplier for temperature dependence of sediment ammonium flux	-	1.08	1.04 – 1.10 [A]
$F_{max}^{NO_3}$	maximum flux of nitrate across the sediment water interface	mmol N m^{-2} d^{-1}	5.2	*River:* 4.3 – 12.8 [B] *Estuary:* 5.2 [C]; -7.2 – 7.1 [E]; 0.4 [H]
$K_{sed}^{NO_3}$	half saturation constant for oxygen dependence of sediment nitrate flux	mmol O_2 m^{-3}	100.0	*Estuary:* 100 [C]
$\theta_{sed}^{NO_3}$	temperature multiplier for temperature dependence of sediment nitrate flux	-	$= \theta_{sed}$ =1.08	1.04 – 1.10 [A]
F_{max}^{DON}	maximum flux of dissolved organic nitrogen across the sediment water interface	mmol N m^{-2} d^{-1}	5.2	*River:* 1.28 – 2.20 [B]
K_{sed}^{DON}	half saturation constant for oxygen dependence of sediment dissolved organic nitrogen flux	mmol N m^{-3}	100.0	estimated
θ_{sed}^{DON}	temperature multiplier for temperature dependence of sediment dissolved organic nitrogen flux	-	$= \theta_{sed}$ =1.08	1.04 – 1.10 [A]

Parameters based on the following information:

[A]   Converted from data on oligotrophic lakes (Romero *et al.*, 2004) to eutrophic lakes (Gal *et al.*, 2009), and justifications therein.

[B]   Based on Hipsey *et al.* (2010) ELCOM-CAEDYM model of the lower Murray River); estimated from data from Prof. Justin Brookes.

[C]   Based on Bruce *et al.* (2011) GETM-FABM-AED application on the Yarra Estuary (Victoria); estimated from data from Roberts *et al.* (2013).

[D]   Net flux measured during eddy correlation experiment in the Upper Swan Estuary (Department of Water, unpublished data); varied in the range 20 – 150 mmol O_2/m^2/d with a background concentration of 260 mmol O_2/m^3, therefore $F_{max}^{O_2}$ ~ 50/(260/(260+150)) = 79 mmol O_2/m^2/d.

[E]   Based on benthic chamber studies showing an average net flux of 50 mmol O_2/m^2/d the Upper Swan estuary (Smith *et al.*, 2007).

[F]   Based on Smith *et al.*, (2007) assessment of data from the Upper Swan estuary, limitation at low oxygen concentrations is not observed

[G]   Based on Fisher *et al.*, (2005) benthic fluxes in Lake Okeechobee

[H]   Based on Crowe *et al.*, (2012) Table 4 synthesis and measurements of N flux in St Lawrence Estuary

Phytoplankton

Empirical work on the Swan Estuary

The estuary has a highly seasonal hydrology and typical successions of various phytoplankton species are observed throughout the year (Thomson and Hosja, 1996; Chan and Hamilton, 2001; Brearley and Hodgkin, 2005). Increased nutrient inputs in freshwater runoff has caused the Swan River Estuary to become progressively eutrophic (Thomson 1998), and in particular, the phytoplankton dynamics in the upper estuary reaches (~20 to 40km from the mouth) have become a concern due to frequent blooms of problematic phytoplankton species. A bloom of the blue-green alga *Microcystis aeruginosa* (Robson and Hamilton, 2003) following summer rains was also of particular concern in terms of its impacts on the river amenity and long-term health of the ecosystem. A sudden bloom of *Karlodinium* in 2003 caused massive fish kills in the Swan and Canning rivers. Fish kills associated with *Karlodinium* have occurred in 2003 - 2006, 2010 and 2012, but in other years blooms have occurred and have not killed fish. Fish kills have also occurred in the Canning Estuary (Phytoplankton Ecology Unit, Department of Water).

Like most estuaries, nitrogen has been observed to be the major nutrient limiting the annual production (Thomson and Hosja, 1996) with nitrogen (N) up to 20 times more limiting than phosphorus (P) in mid-summer, presumably due to conversion of inorganic N to N_2 gas through denitrification acting as a net loss. However, variability in nutrients was observed to be less important than flow and salinity in regulating phytoplankton and biomass in some cases and it was noted that the influence of freshwater discharge triggers variability in the dominant species assemblages and phytoplankton bloom formation in the Upper Swan Estuary (Hodgkin, 1987; Chan and Hamilton, 2001). However, the use of a coupled hydrodynamic-ecological numerical model to explore the individual and collective impacts of hydrological changes within the SCE indicated that despite increased hydraulic flushing and reduced residence times, increases in nutrient loads were able to produce increases in the incidence and peak biomass of blooms of both estuarine and freshwater phytoplankton. In this case, changes in salinity associated with altered seasonal freshwater discharge were reported to have a limited impact on overall phytoplankton abundance (Chan et al., 2002). Other studies of the long-term, phytoplankton species have also had trouble identifying predictable trends in species biomass and timing.

Specific analysis of data during the 2000 *Microcystis* bloom showed that salinity and temperature were the primary factors controlling the growth of this species during this bloom period (Robson and Hamilton, 2004), which occurred when a P rich pulse of fresh warm water occurred after a summer storm. Perhaps a more significant management challenge over recent years however is the presence of nuisance dinoflagellates. Specifically, the physiological requirements of *K. veneficum* isolated from the SCE have been studied and shown to have a wide tolerance of salinity showing growth from 15 - 35 ppt (Hallegraeff et al., 2011). They prefer warm water (17 - 20°C), with a maximum tolerance of ~25°C. In addition, it has been shown to have mixotrophic feeding ability and was also able to grow phototrophically (0.2 - 0.8 divisions d^{-1}) (Adolf et al., 2008; Hallegraeff et al., 2011). However, mixotrophic feeding only happens under conditions of phosphorus deficiency and when there is a high availability of prey, which has been demonstrated to increase its stationary phase of growth under P-limited conditions (Mooney et al., 2010). An early study by Griffin et al. (2001) showed zooplankton to be potentially important in attenuating a dinoflagellate bloom that occurred over a 3-week model simulation period, however this has yet to be supported empirically. Work undertaken by Gedaria et al. (2013) also highlighted the potential contribution of picophytoplankton to estuarine productivity, and demonstrated the ubiquitous presence of the small cyanobacteria *Synechoccoccus*. In addition, a detailed multivariate ordination of all picoplankton and microplankton data collected throughout 2009 was undertaken to determine their response to the various environmental conditions.

Therefore, whilst both large variability in salinity, nutrient levels and light climate have each been postulated to be the primary control on phytoplankton niche and bloom formation, the most appropriate summary was made by Hamilton et al. (2006), who stated that the "conditions that favour bloom occurrence were not due to a single limiting factor, but rather a coalescence of variable factors", thus making targeted management actions difficult.

Model approach

The approach to simulate algal biomass is to adopt several plankton functional types (PFTs) that are typically defined based on specific groups such as diatoms, dinoflagellates and cyanobacteria. Whilst each group that is simulated is unique, they share a common mathematical approach and each simulate growth, death and sedimentation processes,

and customisable internal nitrogen, phosphorus and/or silica stores if desired. Distinction between groups is made by adoption of groups specific parameters for environmental dependencies, and/or enabling options such as vertical migration or N fixation.

The algal biomass of each group, PHY_C, is simulated in units of carbon (mmol C m^{-3}), and the group can be configured to have a constant C:N:P:Si ratio, or have dynamic uptake of N and P sources in response to changing water column condition and cellular physiology. Balance equations that capture the various processes impacting phytoplankton are outlined in Table 8.

Table 13: Mass balance and functions related to the phytoplankton model.

State variable mass balance equations:

Carbon

$$\frac{d(PHY_{C_a})}{dt} = +f_{uptake}^{PHY_{C_a}} - f_{excr}^{PHY_{C_a}} - f_{mort}^{PHY_{C_a}} - f_{resp}^{PHY_{C_a}} - f_{sett}^{PHY_{C_a}} - \sum_z^{N_{ZOO}} (f_{assim}^z\, p_a^z) \tag{45}$$

Nitrogen

$$\frac{d(PHY_{N_a})}{dt} = +f_{uptake}^{PHY_{N_a}} - f_{excr}^{PHY_{N_a}} - f_{mort}^{PHY_{N_a}} - f_{sett}^{PHY_{N_a}} - \sum_z^{N_{ZOO}} \left(f_{assim}^z\, p_a^z\, \frac{PHY_{N_a}}{PHY_{C_a}}\right) \tag{46}$$

Phosphorus

$$\frac{d(PHY_{P_a})}{dt} = +f_{uptake}^{PHY_{P_a}} - f_{excr}^{PHY_{P_a}} - f_{mort}^{PHY_{P_a}} - f_{sett}^{PHY_{P_a}} - \sum_z^{N_{ZOO}} \left(f_{assim}^z\, p_a^z\, \frac{PHY_{P_a}}{PHY_{C_a}}\right) \tag{47}$$

Silica

$$\frac{d(PHY_{Si_a})}{dt} = +f_{uptake}^{PHY_{Si_a}} - f_{excr}^{PHY_{Si_a}} - f_{sett}^{PHY_{Si_a}} - \sum_z^{N_{ZOO}} \left(f_{assim}^z\, p_a^z\, \frac{PHY_{Si_a}}{PHY_{C_a}}\right) \tag{48}$$

= + uptake (C,N,P & Si)
 – excretion
 – mortality
 – **vertical movement** (settling or migration)
 – **grazing losses**

Diagnostic & derived outputs:

Chlorophyll-a

$$TCHLA = \sum_a^{N_{PHY}} \left\{\chi_{C:Chla}^{PHY_a}\, PHY_{C_a}\right\} \tag{49}$$

Gross-primary production

$$GPP = \sum_a^{N_{PHY}} \left\{\chi_{C:Chla}^{PHY_a}\, PHY_{C_a}\right\} \tag{50}$$

Process summary: Photosynthesis and nutrient uptake

For each phytoplankton group, the maximum potential growth rate at 20°C is multiplied by the minimum value of expressions for limitation by light, phosphorus, nitrogen and silica (when configured). While there may be some interaction between limiting factors, a minimum expression is likely to provide a realistic representation of growth limitation (Rhee and Gotham, 1981).

Therefore, photosynthesis is parameterized as the uptake of carbon, and depends on the temperature, light and nutrient dimensionless functions (adopted from Hipsey & Hamilton, 2008; Li et al., 2013).

$$f_{uptake}^{PHY_{Ca}} = \underbrace{R_{growth}^{PHY_a}}_{\substack{\text{max growth} \\ \text{rate at 20C}}} \underbrace{\left(1 - k_{pr}^{PHY_a}\right)}_{\substack{\text{photorespiratory} \\ \text{loss}}} \underbrace{\Phi_{tem}^{PHY_a}(T)}_{\substack{\text{temperature} \\ \text{scaling}}} \underbrace{\Phi_{str}^{PHY_a}(X)}_{\substack{\text{metabolic} \\ \text{stress}}} \dots$$

$$\dots \min \left\{ \underbrace{\Phi_{light}^{PHY_a}(I)}_{\text{light limitation}}, \underbrace{\Phi_{N}^{PHY_a}(NO_3, NH_4, PHY_{N_a})}_{\text{N limitation}}, \underbrace{\Phi_{P}^{PHY_a}(PO_4, PHY_{P_a})}_{\text{P limitation}}, \underbrace{\Phi_{Si}^{PHY_a}(RSi)}_{\text{Si limitation}} \right\} [PHY_{Ca}] \qquad (51)$$

To allow for reduced growth at non-optimal temperatures, a temperature function is used where the maximum productivity occurs at a temperature T_{OPT}; above this productivity decreases to zero at the maximum allowable temperature, T_{MAX}. Below the standard temperature, T_{STD} the productivity follows a simple Arrehenius scaling formulation. In order to fit a function with these restrictions the following conditions are assumed: at $T = T_{STD}$, $\Phi_{tem}(T)=1$ and at $T = T_{OPT}$, $\frac{d\Phi_{tem}(T)}{dT} = 0$, and at $T = T_{MAX}, \Phi_{tem}(T) = 0$. This can be numerically solved using Newton's iterative method and can be specific for each phytoplankton group. The temperature function is calculated according to (Griffin et al. 2001):

$$\Phi_{tem}^{PHY_a}(T) = \vartheta_a^{T-20} - \vartheta_a^{k[T-c1_a]} + c0_a \qquad (52)$$

where $c1_a$ and $c0_a$ are solved numerically given input values of: T_a^{std}, T_a^{opt} and T_a^{max}.

The level of light limitation on phytoplankton growth can be modelled as photoinhibition or non-photoinhibition. In the absence of significant photoinhibition, Webb et al. (1974) suggested a relationship for the fractional limitation of the maximum potential rate of carbon fixation for the case where light saturation behaviour was absent (Talling, 1957), and the equations can be analytically integrated with respect to depth (Hipsey and Hamilton, 2008). For the case of photoinhibition, the light saturation value of maximum production (I_S) is used and the net level effect can be averaged over the cell by integrating over depth.

The `aed_phytoplankton` module contains several light functions, including those from a review by Baklouti et al. (2006). The user must select the sensitivity to light according to a photosynthesis-irradiance (P-I curve) formulation and each species must be set to be either non-photoinhibited or photoinhibited according to the options in Table 9.

Table 14: Selection of P-I functions available for selection for each species in `aed_phytoplankton`.

$\Phi_{light}^{PHY_a}(I) =$			
$1 - e^{\left(-\frac{I}{I_{K_a}}\right)}$	$\Theta_{Light}^{PHY_a} = 0$	Non-photoinhibited	Webb et al. (1974), with numerical integration over depth as in CAEDYM (Hipsey and Hamilton, 2008)
$\dfrac{\left(\frac{I}{I_{K_a}}\right)}{1 + \left(\frac{I}{I_{K_a}}\right)}$	$\Theta_{Light}^{PHY_a} = 1$	Non-photoinhibited	Monod (1950)
$\dfrac{I}{I_{S_a}} e^{\left(1 - \frac{I}{I_{S_a}}\right)}$	$\Theta_{Light}^{PHY_a} = 2$	Photoinhibited	Steele (1962)
$1 - e^{\left(-\frac{I}{I_{K_a}}\right)}$	$\Theta_{Light}^{PHY_a} = 3$	Non-photoinhibited	Webb et al. (1974)
$tanh\left(\dfrac{I}{I_{K_a}}\right)$	$\Theta_{Light}^{PHY_a} = 4$	Non-photoinhibited	Jassby and Platt (1976)
$\dfrac{e^{\left(\frac{I}{I_{K_a}} + \epsilon\right)} - 1}{e^{\left(\frac{I}{I_{K_a}} + \epsilon\right)} + \epsilon}$	$\Theta_{Light}^{PHY_a} = 5$	Non-photoinhibited	Chalker (1980); $\epsilon \sim 0.5$
$\dfrac{(2 + A)\left(\frac{I}{I_{S_a}}\right)}{1 + A\left(\frac{I}{I_{S_a}}\right) + \left(\frac{I}{I_{S_a}}\right)^2}$	$\Theta_{Light}^{PHY_a} = 6$	Photoinhibited	Ebenhoh et al. (1997); A ~ 5.

Limitation of the photosynthetic rate may be dampened according to nitrogen or phosphorus availability, and this is either approximated using a Monod expression of the static model is chosen, or based on the internal nutrient stoichiometry if the dynamic (Droop uptake) model is selected:

For advanced users, an optional metabolic scaling factor can be included to reduce the photosynthetic capacity of the simulated organisms, for example due to metabolic stress due to undertaking N_2 fixation:

$$\Phi_{str}^{PHY_a} = \underbrace{f_{NF}^{PHY_a} + [1 - f_{NF}^{PHY_a}]\Phi_N^{PHY_a}(NO_3, NH_4, PHY_{N_a})}_{N_2 \text{ fixation growth scaling}} \tag{53}$$

The above discussion relates to photosynthesis and carbon uptake by the phytoplankton community. In addition users must choose one of two options to model the P, N uptake dynamics for each algal group: a constant nutrient to carbon ratio, or dynamic intracellular stores. For the first model a simple Michaelis-Menten equation is used to model nutrient limitation with a half-saturation constant for the effect of external nutrient concentrations on the growth rate.

The internal phosphorus and nitrogen dynamics within the phytoplankton groups can be modelled using dynamic intracellular stores that are able to regulate growth based on the model of Droop (1974). This model allows for the phytoplankton to have dynamic nutrient uptake rates with variable internal nutrient concentrations bounded by user-defined minimum and maximum values (e.g., see Li *et al.*, 2013).

Table 15: N, P and Si phytoplankton uptake rate functions.

$f_{uptake}^{PHY_{N_a}}$			
$f_{uptake}^{PHY_{C_a}} \Big/ \chi_{C:N}^{PHY_a}$	$\Theta_{NUptake}^{PHY_a} = 0,1$	Static uptake rate	-
$R_{NUptake}^{PHY_a}\ \Phi_{tem}^{PHY_a}(T)\left\{\Phi_N^{PHY_a}\dfrac{\left(\frac{[PHY_{N_a}]}{[PHY_{C_a}]} - \chi_{NMIN}^{PHY_a}\right)}{\left(\chi_{NMAX}^{PHY_a} - \chi_{NMIN}^{PHY_a}\right)}\right\}PHY_{N_a}$	$\Theta_{NUptake}^{PHY_a} = 2$	Dynamic uptake rate	Hipsey and Hamilton (2008)
$f_{uptake}^{PHY_{P_a}}$			
$f_{uptake}^{PHY_{C_a}} \Big/ \chi_{C:P}^{PHY_a}$	$\Theta_{PUptake}^{PHY_a} = 0,1$	Static uptake rate	-
$R_{PUptake}^{PHY_a}\ \Phi_{tem}^{PHY_a}(T)\left\{\Phi_P^{PHY_a}\dfrac{\left(\frac{[PHY_{P_a}]}{[PHY_{C_a}]} - \chi_{PMIN}^{PHY_a}\right)}{\left(\chi_{PMAX}^{PHY_a} - \chi_{PMIN}^{PHY_a}\right)}\right\}[PHY_{P_a}]$	$\Theta_{PUptake}^{PHY_a} = 2$	Dynamic uptake rate	Hipsey and Hamilton (2008)
$f_{uptake}^{PHY_{Si_a}}$			
$f_{uptake}^{PHY\_C_a} \Big/ \chi_{C:Si}^{PHY_a}$		Static uptake rate	-

The uptake of nitrogen must be partitioned into uptake of NO_3, NH_4 and potentially labile DON. In the present version, distinction between uptake of NO_3 and NH_4 is calculated automatically via a preference factor:

$$p_{NH4}^{PHY_a} = \frac{NO_3\ NH_4}{\left(NH_4 + K_N^{PHY_a}\right)\left(NO_3 + K_N^{PHY_a}\right)}\frac{NH_4\ K_N^{PHY_a}}{\left(NH_4 + NO_3\right)\left(NO_3 + K_N^{PHY_a}\right)} \tag{54}$$

$$p_{NO3}^{PHY_a} = 1 - p_{NH4}^{PHY_a}$$

For diatom groups, silica processes are simulated that include uptake of dissolved silica. The silica limitation function for diatoms is similar to the constant cases for nitrogen and phosphorus which assumes a fixed C:Si ratio.

Process summary: Respiration, excretion and mortality

Metabolic loss of nutrients from mortality and excretion is proportional to the internal nitrogen to chl-a ratio multiplied by the loss rate and the fraction of excretion and mortality that returns to the detrital pool. Loss terms for respiration, natural mortality and excretion are modelled with a single 'respiration' rate coefficient. This loss rate is then divided into the pure respiratory fraction and losses due to mortality and excretion. The constant f_{DOM} is the fraction of mortality and excretion to the dissolved organic pool with the remainder into the particulate organic pool.

Nutrient losses through mortality and excretion for the internal nutrient model are similar to the simple model described above, except that dynamically calculated internal nutrient concentrations are used.

$$\hat{R} = R_{resp}^{PHY_a} \; \Phi_{sal}^{PHY_a}(S) \; \left(\vartheta_{resp}^{PHY_a}\right)^{T-20} \tag{55}$$

$$f_{resp}^{PHY_{C_a}} = k_{fres}^{PHY_a} \, \hat{R} \, \left[PHY_{C_a}\right] \tag{56}$$

$$f_{excr}^{PHY_{C_a}} = \left(1 - k_{fres}^{PHY_a}\right) k_{fdom}^{PHY_a} \, \hat{R} \, \left[PHY_{C_a}\right] \tag{57}$$

$$f_{mort}^{PHY_{C_a}} = \left(1 - k_{fres}^{PHY_a}\right) \left(1 - k_{fdom}^{PHY_a}\right) \hat{R} \, \left[PHY_{C_a}\right] \tag{58}$$

$$f_{excr}^{PHY_{N_a}} = k_{fdom}^{PHY_a} \, \hat{R} \, \left[PHY_{N_a}\right] \tag{59}$$

$$f_{mort}^{PHY_{N_a}} = \left(1 - k_{fdom}^{PHY_a}\right) \hat{R} \, \left[PHY_{N_a}\right] \tag{60}$$

$$f_{excr}^{PHY_{P_a}} = k_{fdom}^{PHY_a} \, \hat{R} \, \left[PHY_{P_a}\right] \tag{61}$$

$$f_{mort}^{PHY_{P_a}} = \left(1 - k_{fdom}^{PHY_a}\right) \hat{R} \, \left[PHY_{P_a}\right] \tag{62}$$

$$f_{excr}^{PHY_{Si_a}} = \hat{R} \, \left[PHY_{Si_a}\right] \tag{63}$$

The salinity effect on mortality is given by various quadratic formulations, depending on the groups sensitivity to salinity (Griffin et al 2001; Robson and Hamilton, 2004). An example of the use of various salinity limitation options is shown in Figure 5.

Table 16: Respiration multiplier as a function of salinity.

| $\Phi_{sal}^{PHY_a}(S) =$			(64)
1		$\Theta_{SalTol}^{PHY_a} = 0$	No salinity effect
$\begin{cases} 1 & \text{if } S < S_{opt}^{PHY_a} \\ 1 + \dfrac{\left(S_{bep}^{PHY_a} - 1\right) S^2}{\left(S_{max}^{PHY_a} - S_{opt}^{PHY_a}\right)^2} - \dfrac{2\left(S_{bep}^{PHY_a} - 1\right) S_{opt}^{PHY_a} S}{\left(S_{max}^{PHY_a} - S_{opt}^{PHY_a}\right)^2} + \dfrac{\left(S_{bep}^{PHY_a} - 1\right)\left(S_{opt}^{PHY_a}\right)^2}{\left(S_{max}^{PHY_a} - S_{opt}^{PHY_a}\right)^2} & \text{if } S > S_{opt}^{PHY_a} \end{cases}$		$\Theta_{SalTol}^{PHY_a} = 1$	Freshwater species
$\begin{cases} 1 & \text{if } S < S_{opt}^{PHY_a} \\ \dfrac{\left(S_{bep}^{PHY_a} - 1\right) S^2}{\left(S_{opt}^{PHY_a}\right)^2} - \dfrac{2\left(S_{bep}^{PHY_a} - 1\right) S}{\left(S_{opt}^{PHY_a}\right)^2} & \text{if } S > S_{opt}^{PHY_a} \end{cases}$		$\Theta_{SalTol}^{PHY_a} = 2$	Marine species
$\begin{cases} 1 & \text{if } S < S_{opt}^{PHY_a} \\ S_{bep}^{PHY_a} + \dfrac{\left(S_{bep}^{PHY_a} - 1\right) S^2}{\left(S_{opt}^{PHY_a}\right)^2} - \dfrac{2\left(S_{bep}^{PHY_a} - 1\right) S}{\left(S_{opt}^{PHY_a}\right)^2} & \text{if } S > S_{opt}^{PHY_a} \end{cases}$		$\Theta_{SalTol}^{PHY_a} = 3$	Estuarine species
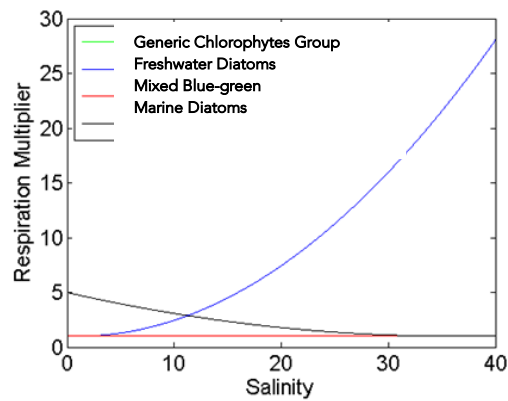
Figure 5. Example of salinity response functions, $\Phi_{sal}^{PHY}(S)$, for four phytoplankton groups being simulated within a river-estuary model. This example demonstrates how fresh, estuarine and marine species can be incorporated together.

Group selection and parameter justification

Simulating too many plankton groups is notoriously difficult (e.g., see Shimoda and Arhonditsis, 2016) and the level of predictability reduces after four or five species unless clear environmental cues are known to drive shifts in community structure. Numerous prior efforts have been undertaken to establish the typical pattern of phytoplankton dominance in the Swan including a conceptual model in Brearley and Hodgkin (2005) and work by Gedaria et al. (2013), in addition to the studies outlined above. By grouping microscopic counts into functional groups, we prepared an overview of seasonal and spatial changes in the Swan (Figure 6).

In line with the typically reported phytoplankton concentrations by the Department of Water, the model is to be configured to simulate 5 discrete groups of phytoplankton that are representative of:

- **Greens (GREEN)** - generic group of chlorophytes where cells contain chlorophyll a and b. This group of algae is extremely diverse, and includes both freshwater and marine representatives. *Chlamydomonas*, *Pyramimonas* and *Carteria* are good representation of the basic chlorophyte species commonly present in the Swan all year round. Distinctive groups of freshwater chlorophytes include groups of cells of a characteristic number and shape. Examples of freshwater chlorophytes observe in the Upper Swan includes *Ankistrodesmus*, *Chlamydomonas globosa*, *Micractinium* and *Golenkinia.*
- **Diatoms (DIATOM)** - marine diatoms are usually the most abundant group observed long in the estuary. Most marine diatoms observed in the lower to middle reaches of the estuary are centric diatoms. Typical species include *Skeletonema costatum*, *Cyclotella*, *Thalassiosira* and *Chaetoceros. Cylindrotheca closterium* is usually abundant in the upper reaches and coming from Avon River. Freshwater diatoms also occur, including *Melosira* in the middle to upper reaches when there is freshwater input in the estuary and larger Naviculoid cells also occur occasionally. In the Canning River where freshwater salinities are commonly observed, *Aulacoseira granulata* is most abundant. As seen in the below tables the is not a striking separation of marine and freshwater species and so these groups are lumped into a common diatom pool in the model.
- **Blue Greens (BGA)** – the presence of cyanobacteria species in the Swan are relatively low, and usually denotes freshwater influence into the estuary and with some groups coming from the small catchments in the middle to upper reaches, as well as Avon River. Species observed includes *Oscillatoria*, *Microcystis*, *Anabaena*, *Pseudanabaena* and *Anabaenopsis*. Additionally, Gedaria and Hipsey (2013) has reported extensive distribution of the picocyanobacteria *Synechococcus*, which is also lumped into this group.
- **Dinoflagellates (DINO)** – A range of dinoflagellates occur throughout the estuary, including *Gymnodinium*, *Gyrodinium*, *Heterocapsa*, *Scripsiella*, and *Prorocentrum. Karlodinium* in particular is a bloom forming and nuisance species in Swan River causing massive fish kills, although it is less dominant than other species in terms of biomass. This species is usually most abundant in brackish salinity during summer to autumn.
- **Cryptophytes (CRYPT)** - this group captures the cryptophytes within the system, which include *Plagioselmis*, *Cryptomonas* and generic small cryptophytes.

Table 17: Summary of the dominant phytoplankton species by cell count, identified and quantified for each season and sampling site, as measured in 2009 by Gedaria et al. (2013). Colour shading used to highlight functional groups of the model.

Site	Summer	Autumn	Winter	Spring
BLA	Thalassiosira (MDIAT) 16.92%	Skeletonema costatum (MDIAT) 61.81%	Skeletonema costatum (MDIAT) 85.38%	Skeletonema costatum (MDIAT) 57.58%)
	Chlamydomonas (GRN) 11.10%	Chaetoceros (chains) (MDIAT) 13.62%	Cyclotella (MDIAT) 4.38%	Chaetoceros (chains) (MDIAT) 15.58%)
	Cylindrotheca closterium (MDIAT) 9.10%	Chaetoceros curvateus (MDIAT) 7.14%	Plagioselmis (DINO) 3.22%	Cyclotella / Thalassiosira (MDIAT) 8.10%)
	Gymnodinium (small) (DINO) 8.69%	Cylindrotheca closterium (MDIAT) 4.78%	Cyclotella / Thalassiosira (MDIAT) 1.40%	Gymnodinium (small) (DINO) 6.11%)
	Chaetoceros (single) (MDIAT) 7.01%	Plagioselmis (DINO) 2.61%	small cryptophytes (DINO) 1.20%	Cyclotella (MDIAT) 2.78%)
	Skeletonema costatum (MDIAT) 6.73%	Gymnodinium (small) (DINO) 1.82%	Gymnodinium (small) (DINO) 1.01%	small cryptophytes (DINO) 2.11%)
	Heterocapsa (<10um) (DINO) 4.34%	Cyclotella / Thalassiosira (MDIAT) 1.18%	Heterocapsa (<10um) (DINO) 0.51%	Plagioselmis (DINO) 1.65%)
	Cyclotella / Thalassiosira (MDIAT) 3.94%	passive chlorophyte (<3um) (GRN) 1.04%	Pyramimonas (GRN) 0.37%	Chaetoceros (single) (MDIAT) 1.33%)
	Thalassionema (MDIAT) 3.67%	Naviculoid (>10um) (FDIAT) 0.79%	Heterocapsa (>10um) (DINO) 0.32%	Gymnodinium (Medium) (DINO) 0.96%)
	Katodinium (small) (DINO) 3.41%	small cryptophytes (DINO) 0.69%	Apedinella spinifera (DINO) 0.31%	Ankistrodesmus (GRN) 0.83%)
ARM	Thalassionema (MDIAT) 17.54%	Skeletonema costatum (MDIAT) 64.62%	Skeletonema costatum (MDIAT) 71.95%	Skeletonema costatum (MDIAT) 48.99%)
	Gymnodinium (small) (DINO) 11.97%	Chaetoceros (chains) (MDIAT) 11.11%	Cyclotella (MDIAT) 7.78%	Chaetoceros (chains) (MDIAT) 17.77%)
	Chlamydomonas (GRN) 9.82%	Gymnodinium (small) (DINO) 2.69%	Plagioselmis (DINO) 5.75%	others (Hetero/Gymno - shrunk) (DINO) 9.54%)
	Skeletonema costatum (MDIAT) 8.52%	Prorocentrum dentatum (DINO) 2.50%	Pyramimonas (GRN) 2.62%	Gymnodinium (small) (DINO) 5.46%)
	Cylindrotheca closterium (MDIAT) 6.96%	Chaetoceros curvateus (MDIAT) 2.46%	Heterocapsa (<10um) (DINO) 2.60%	Cyclotella (MDIAT) 5.14%)
	Chaetoceros (single) (MDIAT) 6.05%	Cylindrotheca closterium (MDIAT) 2.22%	Cyclotella / Thalassiosira (MDIAT) 1.96%	Cyclotella / Thalassiosira (MDIAT) 2.73%)
	Thalassiosira (MDIAT) 5.60%	others (Hetero/Gymno - shrunk) (DINO) 2.14%	Gymnodinium (small) (DINO) 1.77%	Plagioselmis (DINO) 2.25%)
	Prorocentrum dentatum (DINO) 5.19%	Plagioselmis (DINO) 1.96%	small cryptophytes (DINO) 0.89%	small cryptophytes (DINO) 2.00%)
	Cyclotella / Thalassiosira (MDIAT) 4.28%	Cyclotella / Thalassiosira (MDIAT) 1.45%	Scrippsiella trochoidea (DINO) 0.61%	Ankistrodesmus (GRN) 1.09%)
	Ceratium furca (DINO) 2.56%	Heterocapsa (<10um) (DINO) 1.10%	Apedinella spinifera (DINO) 0.59%	Gymnodinium (Medium) (DINO) 0.65%)
NAR	Skeletonema costatum (MDIAT) 84.90%	Prorocentrum dentatum (DINO) 59.56%	Skeletonema costatum (MDIAT) 33.61%	Gymnodinium (small) (DINO) 35.12%)
	Gymnodinium (small) (DINO) 2.48%	Gymnodinium (small) (DINO) 7.56%	small cryptophytes (DINO) 17.91%	Skeletonema costatum (MDIAT) 28.81%)
	Chlamydomonas (GRN) 1.80%	Gymnodinium (Medium) (DINO) 4.53%	Gymnodinium (small) (DINO) 16.22%	Gymnodinium (Medium) (DINO) 5.42%)
	passive chlorophyte (<3um) (GRN) 1.71%	Skeletonema costatum (MDIAT) 4.37%	Cyclotella (MDIAT) 14.73%	Scrippsiella trochoidea (DINO) 4.90%)
	Cylindrotheca closterium (MDIAT) 1.62%	GKC (DINO) 3.92%	Cyclotella / Thalassiosira (MDIAT) 7.49%	small cryptophytes (DINO) 3.70%)
	Cyclotella / Thalassiosira (MDIAT) 1.39%	Plagioselmis (DINO) 3.17%	Cylindrotheca closterium (MDIAT) 1.50%	Heterocapsa (<10um) (DINO) 3.43%)
	Scrippsiella trochoidea (DINO) 0.84%	Cyclotella / Thalassiosira (MDIAT) 1.94%	Gymnodinium (Medium) (DINO) 1.43%	Cyclotella / Thalassiosira (MDIAT) 3.21%)
	Gymnodinium (Medium) (DINO) 0.73%	others (Hetero/Gymno - shrunk) (DINO) 1.88%	Naviculoid (>10um) (FDIAT) 1.09%	others (Hetero/Gymno - shrunk) (DINO) 2.44%)
	Thalassionema (MDIAT) 0.71%	Scrippsiella trochoidea (DINO) 1.74%	Plagioselmis (DINO) 1.01%	Cyclotella (MDIAT) 2.34%)
	Chaetoceros (single) (MDIAT) 0.51%	Cylindrotheca closterium (MDIAT) 1.59%	Oscillatoria (BGA) 0.97%	Plagioselmis (DINO) 1.86%)
STJ	Skeletonema costatum (MDIAT) 66.51%	Prorocentrum dentatum (DINO) 52.59%	Gymnodinium (small) (DINO) 42.41%	Skeletonema costatum (MDIAT) 47.98%)
	Chlamydomonas (GRN) 17.07%	Skeletonema costatum (MDIAT) 17.05%	small cryptophytes (DINO) 23.93%	Plagioselmis (DINO) 13.58%)
	Gymnodinium (small) (DINO) 3.97%	Cyclotella / Thalassiosira (MDIAT) 6.57%	Cyclotella (MDIAT) 9.90%	Cyclotella (MDIAT) 11.17%)
	Euglena (DINO) 3.01%	Plagioselmis (DINO) 4.02%	Cyclotella / Thalassiosira (MDIAT) 7.61%	Gymnodinium (small) (DINO) 11.12%)
	Thalassiosira (MDIAT) 1.75%	Gymnodinium (small) (DINO) 3.32%	Naviculoid (>10um) (FDIAT) 4.31%	Gymnodinium (Medium) (DINO) 2.78%)
	Scrippsiella trochoidea (DINO) 1.61%	Prorocentrum micans (DINO) 2.55%	Cylindrotheca closterium (MDIAT) 2.29%	Cryptomonas (DINO) 2.03%)
	Peridinium (DINO) 0.62%	Gymnodinium (Medium) (DINO) 1.85%	Gymnodinium (Medium) (DINO) 2.16%	Entomoneis (MDIAT) 1.67%)
	Gyrodinium (>10um) (DINO) 0.58%	Scrippsiella trochoidea (DINO) 1.52%	Plagioselmis (DINO) 1.06%	Cyclotella / Thalassiosira (MDIAT) 1.27%)
	Oscillatoria (BGA) 0.58%	Teleaulax (DINO) 1.15%	Navicula sp. (<10um) (FDIAT) 0.98%	Pyramimonas (GRN) 1.10%)
	Naviculoid (>10um) (FDIAT) 0.57%	Euglena (DINO) 1.01%	Skeletonema costatum (MDIAT) 0.87%	Chaetoceros (chains) (MDIAT) 1.07%)
KIN	Chlamydomonas (GRN) 90.75%	Cyclotella / Thalassiosira (MDIAT) 16.80%	Gymnodinium (small) (DINO) 38.09%	Gymnodinium (small) (DINO) 27.03%)
	Euglena (DINO) 2.88%	Gymnodinium (small) (DINO) 13.82%	small cryptophytes (DINO) 26.20%	Cryptomonas (DINO) 13.31%)
	Scrippsiella trochoidea (DINO) 1.91%	Plagioselmis (DINO) 12.69%	Cyclotella (MDIAT) 10.41%	small cryptophytes (DINO) 10.25%)
	Gymnodinium (Medium) (DINO) 1.14%	Pyramimonas (GRN) 10.91%	Cyclotella / Thalassiosira (MDIAT) 7.08%	Gymnodinium (Medium) (DINO) 9.86%)
	Thalassiosira (MDIAT) 1.07%	Prorocentrum dentatum (DINO) 9.21%	Cylindrotheca closterium (MDIAT) 5.15%	Scrippsiella trochoidea (DINO) 9.33%)
	Skeletonema costatum (MDIAT) 0.94%	Euglena (DINO) 4.33%	Plagioselmis (DINO) 4.67%	Naviculoid (>10um) (FDIAT) 6.18%)
	Gymnodinium (small) (DINO) 0.28%	Akashiwo sanguineum (DINO) 3.99%	Naviculoid (>10um) (FDIAT) 3.16%	passive chlorophyte (<3um) (GRN) 5.98%)
	Gyrodinium (>10um) (DINO) 0.13%	Gymnodinium (Medium) (DINO) 3.28%	Navicula sp. (<10um) (FDIAT) 1.33%	Pyramimonas (GRN) 5.39%)
	Heterocapsa (<10um) (DINO) 0.11%	Gyrodinium (>10um) (DINO) 3.05%	Gymnodinium (Medium) (DINO) 0.74%	Plagioselmis (DINO) 2.09%)
	Cyclotella / Thalassiosira (MDIAT) 0.11%	Skeletonema costatum (MDIAT) 2.91%	Pyramimonas (GRN) 0.62%	Cyclotella / Thalassiosira (MDIAT) 1.97%)
SUC	Chlamydomonas (GRN) 89.72%	Cyclotella / Thalassiosira (MDIAT) 43.82%	Gymnodinium (small) (DINO) 44.04%	Cryptomonas (DINO) 31.84%)
	Euglena (DINO) 6.16%	Plagioselmis (DINO) 13.64%	small cryptophytes (DINO) 25.21%	Gymnodinium (small) (DINO) 20.55%)
	Scrippsiella trochoidea (DINO) 2.31%	Teleaulax (DINO) 5.33%	Cyclotella (MDIAT) 9.43%	passive chlorophyte (<3um) (GRN) 10.71%)
	Thalassiosira (MDIAT) 0.73%	Gymnodinium (small) (DINO) 5.32%	Cyclotella / Thalassiosira (MDIAT) 7.10%	Naviculoid (>10um) (FDIAT) 6.43%)
	Skeletonema costatum (MDIAT) 0.21%	Gymnodinium (Medium) (DINO) 4.40%	Cylindrotheca closterium (MDIAT) 6.03%	Gymnodinium (Medium) (DINO) 5.73%)
	Gymnodinium (small) (DINO) 0.20%	Skeletonema costatum (MDIAT) 3.05%	Naviculoid (>10um) (FDIAT) 3.10%	small cryptophytes (DINO) 4.90%)
	Peridinium (DINO) 0.10%	Prorocentrum dentatum (DINO) 2.99%	Navicula sp. (<10um) (FDIAT) 0.84%	Pyramimonas (GRN) 3.36%)
	Cylindrotheca closterium (MDIAT) 0.09%	passive chlorophyte (<3um) (GRN) 2.78%	Synedra (MDIAT) 0.79%	Skeletonema costatum (MDIAT) 2.70%)
	Cyclotella / Thalassiosira (MDIAT) 0.08%	Gyrodinium (>10um) (DINO) 2.32%	Pyramimonas (GRN) 0.60%	Navicula sp. (<10um) (FDIAT) 2.08%)
	Gyrodinium (>10um) (DINO) 0.06%	Navicula sp. (<10um) (FDIAT) 1.91%	Plagioselmis (DINO) 0.57%	Cyclotella (MDIAT) 1.91%)

Table 18: Summary of the dominant phytoplankton species sorted by species biomass for each season and station, as measured in 2009 by Gedaria et al. (2013) and converted to biomass based on C content per cell approximation. Colour shading used to highlight functional groups of the model.

|	Summer	Autumn	Winter	Spring
BLA	Ceratium furca (DINO) 59.63%	Skeletonema costatum (MDIAT) 65.50%	Cyclotella (MDIAT) 67.53%	Skeletonema costatum (MDIAT) 52.43%
	Cyclotella (MDIAT) 12.12%	Gyrodinium (>10um) (DINO) 4.73%	Skeletonema costatum (MDIAT) 28.55%	Cyclotella (MDIAT) 32.30%
	Coscinodiscus (MDIAT) 4.12%	Ceratium furca (DINO) 3.18%	Plagioselmis (DINO) 0.56%	GKC (DINO) 4.12%
	Prorocentrum micans (DINO) 2.97%	Chaetoceros curvateus (MDIAT) 3.17%	GKC (DINO) 0.53%	Polykrikos (DINO) 1.79%
	Prorocentrum dentatum (DINO) 2.39%	GKC (DINO) 3.01%	Cyclotella / Thalassiosira (MDIAT) 0.36%	Scrippsiella trochoidea (DINO) 1.65%
	Katodinium (small) (DINO) 1.88%	passive chlorophyte (<3um) (GRN) 2.61%	Heterocapsa (>10um) (DINO) 0.31%	Cyclotella / Thalassiosira (MDIAT) 1.51%
	Thalassiosira (MDIAT) 1.86%	Protoperidium pentagonum (DINO) 2.59%	Gyrodinium (>10um) (DINO) 0.27%	Chaetoceros (chains) (MDIAT) 1.15%
	Peridinium (DINO) 1.68%	Naviculoid (>10um) (FDIAT) 2.15%	Coscinodiscus (MDIAT) 0.24%	Gymnodinium (small) (DINO) 1.04%
	Naviculoid (>10um) (FDIAT) 1.60%	Peridinium (DINO) 1.74%	Teleaulax (DINO) 0.18%	Peridinium (DINO) 0.71%
	Chlamydomonas (GRN) 1.48%	Teleaulax (DINO) 1.33%	Naviculoid (>10um) (FDIAT) 0.17%	Naviculoid (>10um) (FDIAT) 0.50%
ARM	Ceratium furca (DINO) 41.88%	Skeletonema costatum (MDIAT) 48.23%	Cyclotella (MDIAT) 76.14%	Cyclotella (MDIAT) 56.41%
	Cyclotella (MDIAT) 34.01%	Ceratium furca (DINO) 11.79%	Skeletonema costatum (MDIAT) 15.28%	Polykrikos (DINO) 16.69%
	Coscinodiscus (MDIAT) 3.95%	Gyrodinium (>10um) (DINO) 9.70%	Polykrikos (DINO) 2.16%	Skeletonema costatum (MDIAT) 13.03%
	Gyrodinium (>10um) (DINO) 3.17%	Coscinodiscus (MDIAT) 7.77%	Protoperidium pentagonum (DINO) 1.51%	GKC (DINO) 3.55%
	Peridinium (DINO) 2.60%	Prorocentrum micans (DINO) 4.27%	Gyrodinium (>10um) (DINO) 0.68%	Gyrodinium (>10um) (DINO) 2.25%
	Prorocentrum micans (DINO) 2.30%	Prorocentrum dentatum (DINO) 4.00%	Plagioselmis (DINO) 0.63%	Coscinodiscus (MDIAT) 1.80%
	Prorocentrum dentatum (DINO) 1.47%	GKC (DINO) 2.65%	GKC (DINO) 0.58%	Chaetoceros (chains) (MDIAT) 1.06%
	Thalassionema (MDIAT) 1.11%	Chaetoceros curvateus (MDIAT) 0.98%	Scrippsiella trochoidea (DINO) 0.45%	Scrippsiella trochoidea (DINO) 0.72%
	Naviculoid (>10um) (FDIAT) 1.08%	Protoperidium pentagonum (DINO) 0.93%	Cyclotella / Thalassiosira (MDIAT) 0.31%	Teleaulax (DINO) 0.59%
	GKC (DINO) 1.02%	Cyclotella / Thalassiosira (MDIAT) 0.80%	Teleaulax (DINO) 0.30%	others (Hetero/Gymno - shrunk) (DINO) 0.57%
NAR	Cyclotella (MDIAT) 57.13%	Prorocentrum dentatum (DINO) 33.41%	Cyclotella (MDIAT) 88.68%	Cyclotella (MDIAT) 41.59%
	Skeletonema costatum (MDIAT) 23.32%	GKC (DINO) 21.81%	Skeletonema costatum (MDIAT) 4.53%	Scrippsiella trochoidea (DINO) 11.83%
	GKC (DINO) 2.00%	Skeletonema costatum (MDIAT) 19.88%	Plagioselmis (DINO) 0.98%	Skeletonema costatum (MDIAT) 9.56%
	Rhizosolenia (MDIAT) 1.96%	Akashiwo sanguineum (DINO) 8.16%	Gymnodinium (small) (DINO) 0.73%	Polykrikos (DINO) 8.58%
	Gyrodinium (>10um) (DINO) 1.80%	Gyrodinium (>10um) (DINO) 6.73%	Naviculoid (>10um) (FDIAT) 0.70%	Protoperidium pentagonum (DINO) 7.19%
	Peridinium (DINO) 1.58%	Prorocentrum micans (DINO) 2.38%	Cyclotella / Thalassiosira (MDIAT) 0.69%	GKC (DINO) 6.17%
	Protoperidium pentagonum (DINO) 1.43%	Protoperidium pentagonum (DINO) 1.12%	Prorocentrum micans (DINO) 0.65%	Gymnodinium (small) (DINO) 3.20%
	Gonyaulax (DINO) 1.33%	Scrippsiella trochoidea (DINO) 0.97%	Gyrodinium (>10um) (DINO) 0.59%	Gymnodinium (Medium) (DINO) 1.78%
	Scrippsiella trochoidea (DINO) 0.97%	Cyclotella / Thalassiosira (MDIAT) 0.74%	Protoperidium pentagonum (DINO) 0.49%	Entomoneis (MDIAT) 1.08%
	Naviculoid (>10um) (FDIAT) 0.82%	Gymnodinium (Medium) (DINO) 0.69%	Cryptomonas (DINO) 0.29%	Gyrodinium (>10um) (DINO) 1.02%
STJ	Skeletonema costatum (MDIAT) 22.00%	Skeletonema costatum (MDIAT) 38.72%	Cyclotella (MDIAT) 83.22%	Cyclotella (MDIAT) 79.95%
	Cyclotella (MDIAT) 19.96%	Prorocentrum dentatum (DINO) 29.72%	Prorocentrum micans (DINO) 2.24%	Skeletonema costatum (MDIAT) 7.31%
	Peridinium (DINO) 18.58%	Prorocentrum micans (DINO) 6.88%	Naviculoid (>10um) (FDIAT) 1.92%	Peridinium (DINO) 3.38%
	Gyrodinium (>10um) (DINO) 8.85%	Gyrodinium (>10um) (DINO) 4.10%	Heterocapsa (>10um) (DINO) 1.88%	GKC (DINO) 2.23%
	Alexandrium (DINO) 5.38%	GKC (DINO) 3.98%	Gymnodinium (small) (DINO) 1.55%	Entomoneis (MDIAT) 1.31%
	Chlamydomonas (GRN) 4.81%	Akashiwo sanguineum (DINO) 3.50%	Gyrodinium (>10um) (DINO) 1.23%	Cryptomonas (DINO) 0.93%
	Heterocapsa (<10um) (DINO) 3.08%	Scrippsiella trochoidea (DINO) 2.34%	Tetraselmis (GRN) 0.86%	Plagioselmis (DINO) 0.93%
	Scrippsiella trochoidea (DINO) 2.89%	Protoperidium pentagonum (DINO) 1.90%	Protoperidium pentagonum (DINO) 0.84%	Gyrodinium (>10um) (DINO) 0.77%
	Gymnodinium (small) (DINO) 2.75%	Cyclotella / Thalassiosira (MDIAT) 1.75%	GKC (DINO) 0.82%	Gymnodinium (small) (DINO) 0.73%
	Naviculoid (>10um) (FDIAT) 2.09%	Coscinodiscus (MDIAT) 1.23%	Polykrikos (DINO) 0.80%	Naviculoid (>10um) (FDIAT) 0.53%
KIN	Chlamydomonas (GRN) 36.05%	Polykrikos (DINO) 24.68%	Cyclotella (MDIAT) 89.41%	Cyclotella (MDIAT) 31.16%
	Scrippsiella trochoidea (DINO) 30.27%	Gyrodinium (>10um) (DINO) 14.10%	GKC (DINO) 2.22%	Cryptomonas (DINO) 16.99%
	Cyclotella (MDIAT) 16.16%	Skeletonema costatum (MDIAT) 14.04%	Naviculoid (>10um) (FDIAT) 2.11%	Scrippsiella trochoidea (DINO) 13.99%
	Cryptomonas (DINO) 3.65%	Scrippsiella trochoidea (DINO) 7.80%	Gymnodinium (small) (DINO) 1.44%	Naviculoid (>10um) (FDIAT) 13.95%
	Euglena (DINO) 2.62%	Akashiwo sanguineum (DINO) 7.10%	Cyclotella / Thalassiosira (MDIAT) 0.70%	Gymnodinium (Medium) (DINO) 4.77%
	Prorocentrum cordatum (DINO) 2.17%	Cyclotella (MDIAT) 4.90%	Gyrodinium (>10um) (DINO) 0.69%	Gymnodinium (small) (DINO) 4.04%
	Gyrodinium (>10um) (DINO) 1.55%	Gymnodinium (small) (DINO) 4.17%	Plagioselmis (DINO) 0.66%	GKC (DINO) 3.87%
	Peridinium (DINO) 1.28%	Prorocentrum cordatum (DINO) 3.20%	Cylindrotheca closterium (MDIAT) 0.28%	passive chlorophyte (<3um) (GRN) 1.66%
	Skeletonema costatum (MDIAT) 1.16%	Cyclotella / Thalassiosira (MDIAT) 2.86%	Navicula sp. (<10um) (FDIAT) 0.27%	Navicula sp. (<10um) (FDIAT) 1.49%
	Gymnodinium (Medium) (DINO) 0.82%	Prorocentrum micans (DINO) 2.83%	Oxyrrhis marina (DINO) 0.26%	Entomoneis (MDIAT) 1.27%
SUC	Chlamydomonas (GRN) 50.90%	Prorocentrum cordatum (DINO) 25.31%	Cyclotella (MDIAT) 92.86%	Cyclotella (MDIAT) 33.57%
	Cyclotella (MDIAT) 18.21%	Gyrodinium (>10um) (DINO) 23.00%	Cylindrotheca closterium (MDIAT) 1.71%	Cryptomonas (DINO) 32.91%
	Scrippsiella trochoidea (DINO) 9.66%	Cyclotella / Thalassiosira (MDIAT) 9.17%	Naviculoid (>10um) (FDIAT) 1.34%	Naviculoid (>10um) (FDIAT) 11.14%
	Peridinium (DINO) 8.16%	Skeletonema costatum (MDIAT) 8.97%	Gymnodinium (small) (DINO) 1.21%	GKC (DINO) 4.19%
	Euglena (DINO) 4.09%	Rhizosolenia (MDIAT) 8.09%	GKC (DINO) 0.68%	Gymnodinium (small) (DINO) 2.61%
	Skeletonema costatum (MDIAT) 3.85%	GKC (DINO) 4.29%	Cyclotella / Thalassiosira (MDIAT) 0.51%	passive chlorophyte (<3um) (GRN) 2.40%
	Gyrodinium (>10um) (DINO) 1.10%	Polykrikos (DINO) 3.61%	Gyrodinium (>10um) (DINO) 0.29%	Gymnodinium (Medium) (DINO) 2.33%
	Naviculoid (>10um) (FDIAT) 1.05%	Prorocentrum micans (DINO) 3.34%	Synedra (MDIAT) 0.20%	Peridinium (DINO) 1.80%
	Entomoneis (MDIAT) 0.69%	Gyrodinium (<10um) (DINO) 2.75%	Plagioselmis (DINO) 0.16%	Navicula sp. (<10um) (FDIAT) 1.64%
	GKC (DINO) 0.47%	Scrippsiella trochoidea (DINO) 1.55%	Oxyrrhis marina (DINO) 0.16%	Heterocapsa (>10um) (DINO) 1.35%
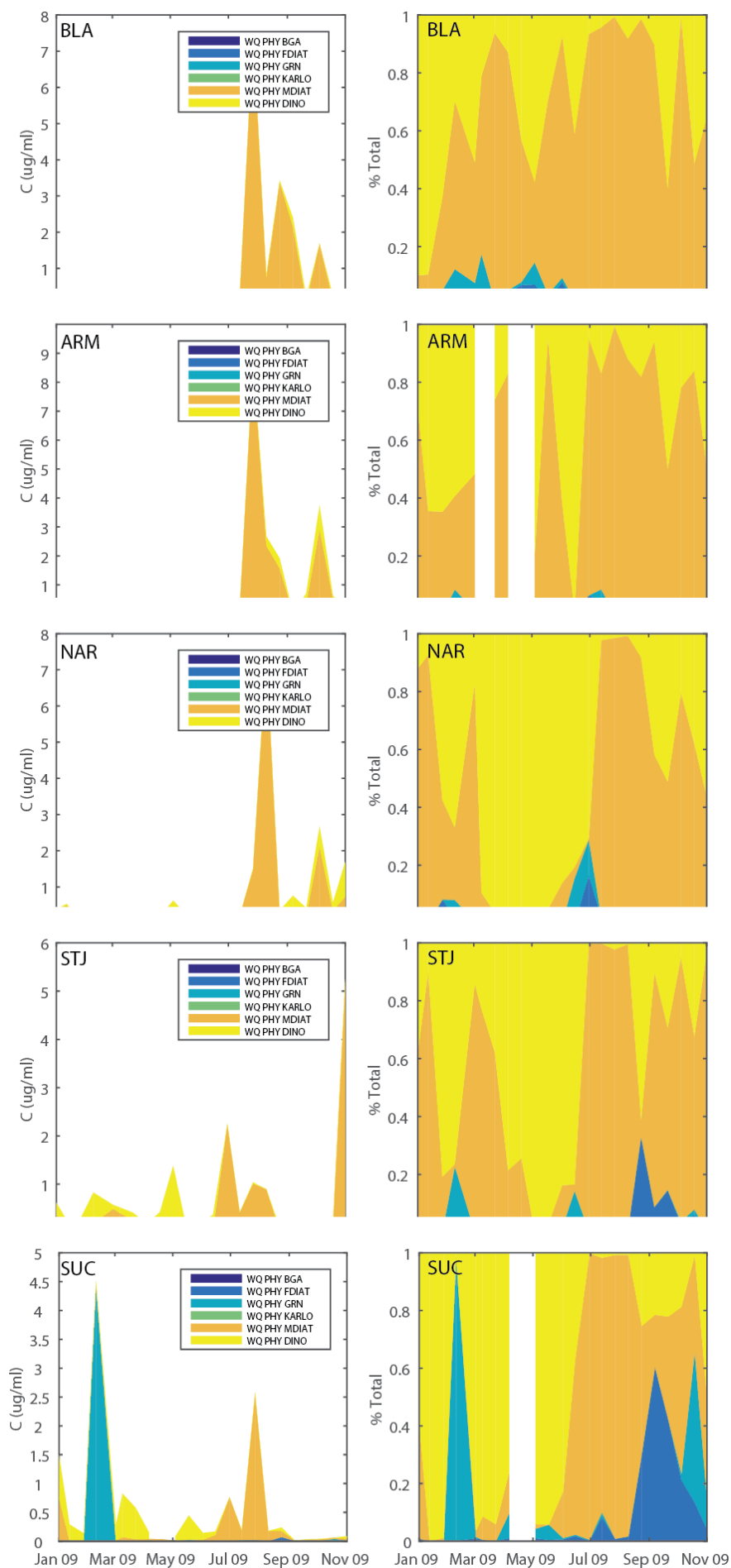
Figure 6. Summary of plankton count groups converted to biomass (left), and as a fraction of total biomass (right).

Table 19: Assumptions used to disaggregate Chl-a into five functional groups. These are qualitatively based on some exploration of correlations in the data in the above tables. BC% indicates the assumed percentage allocated to the specific group from the measured boundary condition Chl-a concentration.

Group	Representative of	Marine (Freo) BC %	Marine (Narrows) BC %	River BC %	Carbon: Chlorophyll	N:P ratio (molar)
		% of Observed Chl-a @ station FREO	% of Observed Chl-a @ station NAR	% of Assumed Chl-a in tributaries	gC/gChla	gN/gP
diatom	Mainly marine diatoms, including *Skeletonema*, *Cyclotella*, *Thalassiosira*, *etc*	80%	55%	15%	26	17:1
dino	Dinoflagellates, including Gymnodinium, *Karlodinium*, *etc*	12%	30%	50%	40	16:1
crypt	Cryptophytes	5%	8%	10%	50	16:1
green	Chlorophytes	2%	4%	15%	50	16:1
bga	Cyanophytes	1%	3%	10%	40	Variable

Table 20: Parameter overview relevant to the Swan-Canning Estuary model configuration.

parameter	description	units	GREEN	BGA	CRYPT	DIATOM	DINO
R_{growth}^{PHY}	phytoplankton growth rate at 20C	d^{-1}	1.3	1.2	1.8	1.55	0.55
I_K	light ½ saturation constant for algal limitation	µE m^{-2} s^{-1}	200	100	200	380	180
K_e^{PHY}	specific attenuation coefficient	mmol C m^{-3} m^{-1}	0.0408	0.0051	0.048	0.048	0.048
ϑ_{growth}^{PHY}	Arrhenius temperature scaling for growth	-	1.06	1.08	1.06	1.07	1.10
T_{std}	standard temperature	C	20	20	18	15	20
T_{opt}	optimum temperature	C	28	28	25	20	25
T_{max}	maximum temperature	C	38	38	37	35	35
R_{resp}^{PHY}	phytoplankton respiration rate at 20C	d^{-1}	0.07	0.08	0.12	0.14	0.05
k_{fres}^{PHY}	fraction of metabolic loss that is respiration	-	0.7	0.7	0.7	0.7	0.7
k_{fdom}^{PHY}	fraction of metabolic loss that is DOM	-	0.3	0.3	0.3	0.3	0.3
ϑ_{resp}^{PHY}	Arrhenius temperature scaling for respiration	-	1.05	1.08	1.08	1.08	1.08
χ_{NCON}^{PHY}	average internal N concentration	mmol N mmol C^{-1}	0.15	0.15	0.15	0.137	0.15
K_N	half-saturation concentration of nitrogen	mmol N m^{-3}	1.786	2.143	2.50	1.60	3.57
$R_{NUptake}^{PHY}$	maximum nitrogen uptake rate	mmol N m^{-3} d^{-1}	0.069	0.032	0.257	0.206	
χ_{NMIN}^{PHY}	minimum internal nitrogen concentration	mmol N mmol C^{-1}	-	0.054	-	-	-
χ_{NMAX}^{PHY}	maximum internal nitrogen concentration	mmol N mmol C^{-1}	-	0.107	-	-	-
χ_{PCON}^{PHY}	average internal P concentration	mmol N mmol C^{-1}	0.0094	0.0094	0.0039	0.0039	0.0094
K_P	half-saturation concentration of phosphorus	mmol P m^{-3}	0.3226	0.1935	0.3226	0.2400	0.161
$R_{PUptake}^{PHY}$	maximum phosphorus uptake rate	mmol P m^{-3} d^{-1}	0.0031	0.0019	0.0015	0.0023	
χ_{PMIN}^{PHY}	minimum internal phosphorus concentration	mmol P mmol C^{-1}	-	0.0039	-	-	-
χ_{PMAX}^{PHY}	maximum internal phosphorus concentration	mmol P mmol C^{-1}	-	0.0077	-	-	-
K_{Si}	half-saturation concentration of silica	mmol Si m^{-3}	8.0	8.0	15.71	3.9	0
$\chi_{C:Si}^{PHY_a}$	internal silicate concentration	mmol Si mmol C^{-1}	0.0171	0.0214	0.01	0.1096	0.01
ω_{PHY}	phytoplankton sedimentation rate	m d^{-1}	-0.1	0	0.0	-0.30	+0.1
S_{opt}^{PHY}	Salinity optimum / limit	ppt	4	1	-	20	23
S_{bep}^{PHY}	Magnitude of salinity effect on mortality rate	-	1	1	0	1	1
S_{max}^{PHY}	Salinity where S_{bep}^{PHY} occurs	ppt	8	15	-	20	26

Parameters based on the following information:

    Cerco and Cole (1993): Chesapeake Bay

    Sarthou et al. (2005): Marine diatoms

    Wild-Allen et al. (2010): Derwent estuary algal modelling

    Robson and Hamilton (2004): Swan Estuary *Microcystis* modelling

    Griffin et al. (2001): Swan Estuary grazing rate estimation

    Chan (2006): Swan Estuary algal modelling

Seagrass habitat

Numerous seagrass coverage surveys have been undertaken for the SCE (Hillman et al., 1995; Forbes and Kilminster, 2014). Meadow coverage is patchy and restricted to the main basin within the lower reaches (see Figure 7), with *Halophila ovalis* being the most prevalent. Simulating seagrass productivity in estuary models has been done by various authors (e.g., Cerco and Moore, 2001; del Barrio et al., 2014), however, it is often relatively simply captured based on a potential rate of photosynthesis relative to respiration (e.g., P/R). More recently, Baird et al. (2016) present an improved mechanistic basis for seagrass simulation, including above:below ground biomass partitioning, and also relating the coverage density with biomass. Nonetheless, despite a relative sophisticated empirical understanding of the controls on seagrass biomass, few studies have successfully attempted to model seagrass meadow dynamics (e.g., meadow expansion or loss) in response to environmental change.
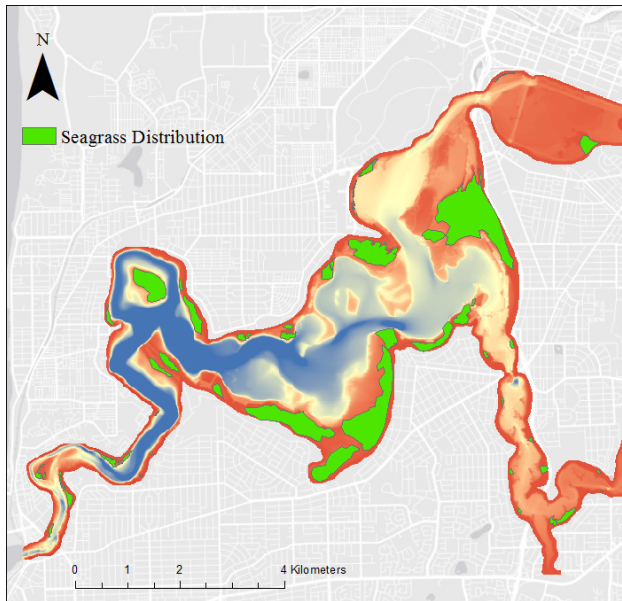
Figure 7. Overview of seagrass coverage in the lower Swan estuary (green), based on 2008 survey data provided by the Department of Water. Colour gradient represents water

We approach the model by including a core state variable *HALO*, that is made up of above ground (AG) and below ground (BG); the former referring to the leaves, and the latter the cumulative mass of rhizomes and roots. The equation for seagrass biomass in a given cell is computed as shown in Table 21, assuming photosynthesis, excretion, mortality and excretion. Nutrient uptake is not included in the simulation in SCERM v1 since Hillman et al. (1995) highlight that light, salinity and temperature were the dominant drivers, with some minor correlation with phosphate levels, however the stoichiometry is known and may be included in future iterations. The effective coverage area (i.e. Leaf Area Index, $HALO_{LAI}$ of the meadow) can be computed based on the scaling expression in Baird et al. (2016); although this is not directly used in the photosynthesis calculation, it is useful output for comparing with field data.

Table 21: Mass balance and functions related to <u>macrophyte (seagrass)</u> growth.

State variable mass balance equations:

$$\frac{d(HALO)}{dt} = +f_{growth}^{MAC} - f_{excr}^{MAC} - f_{mort}^{MAC} - f_{resp}^{MAC} \tag{65}$$

= ± **photosynthesis and growth**
  – **excretion of dissolved organic matter**
  – **leaf mortality and sloughing**
  – **respiration**

$$HALO = HALO_{AG} + HALO_{BG} \tag{66}$$

$$HALO_{LAI} = 1 - exp[-c_{\Omega}(HALO)] \tag{67}$$

Growth is calculated in response to light, but also sensitive to salinity and temperature:

$$f_{growth}^{MAC} = \underbrace{R_{growth}^{MAC_{HALO}}}_{\substack{\text{max growth} \\ \text{rate at 20C}}} \underbrace{\Phi_{tem}^{MAC_{HALO}}(T)}_{\substack{\text{temperature} \\ \text{scaling}}} \underbrace{\Phi_{sal}^{MAC_{HALO}}(S)}_{\substack{\text{salinity} \\ \text{scaling}}} \underbrace{\Phi_{light}^{MAC_{HALO}}(I)}_{\text{light limitation}} \ [HALO] \tag{68}$$

where $R_{growth}^{MAC_{HALO}}$ is the maximum growth rate at 20°C, which changes in response to temperature, salinity and light availability, Φ_{tem}, Φ_{sal} and Φ_{light}. Photosynthesis-irradiance relationships for *Halophila* have been estimated by Ralph and Burchett (1995) who found photo-inhibition occurring at modest light intensities. The Steele (1962) equation (Table 14) is therefore suggested as the most appropriate. Light extinction can also occur over the meadow depth, although for *Halophila* this is assumed to be relatively small due to the small leaf structure. The salinity effect on photosynthesis has been reported by Ralph (1998b) and Hillman et al. (1995).

Respiration, excretion and mortality are also commonly simulated with typical first-order rate coefficients for each:

$$f_{resp}^{MAC} = \underbrace{R_{resp}^{MAC_{HALO}}}_{\substack{\text{respiration} \\ \text{rate at 20C}}} \underbrace{\left(\vartheta_{resp}^{MAC_{HALO}}\right)^{T-20}}_{\substack{\text{temperature} \\ \text{scaling}}} [HALO] \tag{69}$$

$$f_{excr}^{MAC} = \underbrace{k_{excr}^{MAC_{HALO}} \ R_{growth}^{MAC_{HALO}}}_{\substack{\text{excretion} \\ \text{rate at 20C}}} \ [HALO] \tag{70}$$

$$f_{mort}^{MAC} = \underbrace{R_{mort}^{MAC_{HALO}}}_{\substack{\text{mortality} \\ \text{rate at 20C}}} \underbrace{\left(\vartheta_{resp}^{MAC_{HALO}}\right)^{T-20}}_{\substack{\text{temperature} \\ \text{scaling}}} \ [HALO] \tag{71}$$

The seagrass-sediment-light (SSL) feedback has been identified as a potentially important driver determining meadow persistence (Adams et al., 2016), as depicted schematically for a numerical model in Figure 8. This requires the connection between sediment resuspension and seagrass presence to be made, however, the complete feedback loop has rarely been reported in aquatic models to date. The model implemented for SCERM focuses on *Halophila* and accounts for the feedback by including ability to simulate the link between: a) above ground biomass ($HALO_{AG}$) and shear stress, b) below ground biomass ($HALO_{BG}$), and c) the amount of resuspension and light (see Eq 4).
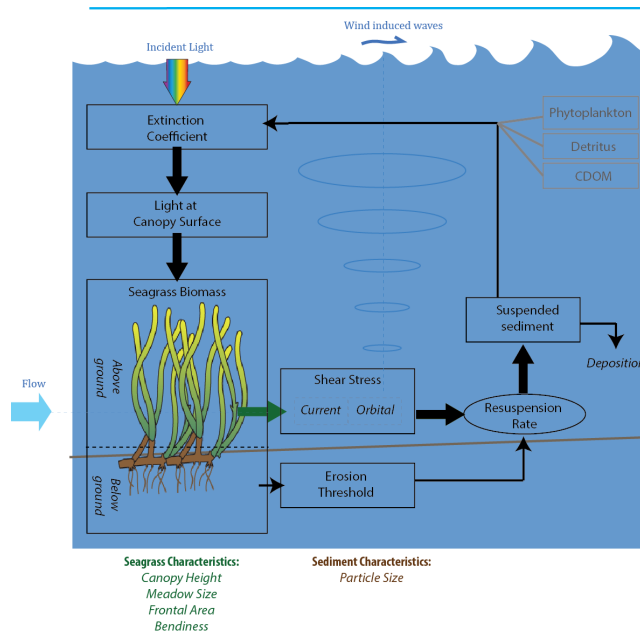

Figure 8. Model approach to capture the sediment-seagrass feedback.

To simulate the SSL feedback, drag is increased in proportion with the above ground biomass:

$$C_D = C_{D_{bottom}} + k_{biodrag}[HALO_{AG}] \tag{72}$$

where C_D is the base drag coefficient for a numerical cell based on its sediment material properties, and the above ground fraction is a user definable constant fraction of total biomass. The default value of $C_{D_{bottom}}$ is stored in the hydrodynamic driver model and influences the local momentum budget; therefore the 2nd term of the RHS is passed to

the host model calling AED2. The critical shear stress for resuspension is also increased based on the below ground biomass:

$$\tau_0 = \tau_{0_{min}} + k_{biotau}[HALO_{BG}] \tag{73}$$

where τ_0 is critical shear stress for resuspension, computed based on a minimum value (reflecting bare sediment), and linear coefficient linked to biomass. As τ_0 increases, the concentration of SS in the local domain will reduce, thereby improving the overall light climate. Note that in the model, presence or absence of $HALO$ in a given cell can be configured be reading in an appropriate distribution map based on Figure 7.

Currently the values of the parameters for *Halophila* come from a range of relevant studies, with several studies reporting productivity response to environmental conditions, however, further research is required to better understand the actual links between *Halophila* biomass and its effect on drag and critical shear stress. References for relevant parameters for *Halophila ovalis* are summarised in Table 22.

Table 22: Seagrass (*Halophila*) model related parameters.

Symbol	Description	Units	Value	Comment
R_{growth}^{PHY}	Maximum growth rate at 20°C	d^{-1}	0.33	*H ovalis:* Hillman et al. (1995) show in SCE net summer productivity of ~15 mg dw apex d^{-1}, and ~ 100 mg apex^{-1} (~15%). Bearing in mind approximately 50% mass partitioning to below ground biomass and ~1000 apices m^{-2}, the net productivity is 30 g m^{-2} d^{-1} which is ~0.33 d^{-1} when normalised by mean biomass of 100 g dw m^{-2}.
I_S	Light intensity for maximum production (before photo-inhibition effects)	uE m^{-2} s^{-1}	300	*H ovalis:* Ralph and Burchett (1995) found inhibition occurring at 500 and 1000 uE m^{-2} s^{-1} Hillman et al. (1995) found optimum at 200 uE m^{-2} s^{-1} in SCE
$K_{e_{MAC}}$	Light attenuation over the depth of the plant (within the canopy)	(m^{-1}) (g m^{-2})$^{-1}$	0	*Assumed to be insignificant*
ϑ_{growth}^{MAC}	Arrhenius temperature scaling for growth	-	1.08	*H ovalis:* Ralph (1998a) found optimum was 25-30°C and no photosynthesis < 12.5 and > 37.5 Hillman et al. (1995) show temperature effect on productivity from 10-25°C in SCE
T_{std}	Standard temperature	C	20	
T_{opt}	Optimum temperature	C	27	
T_{max}	Maximum temperature	C	37	
$k_{ag:bg}^{MAC}$	AG:BG biomass partitioning fraction	-	0.5	*H ovalis:* Hillman et al. (1995) show annual biomass breakdown of leaves roots and rhizomes to be ~50% in SCE
k_{excr}^{MAC}	Macroalgae excretion fraction of photosynthesis	-	0.1	*Assumed*
R_{resp}^{MAC}	Macroalgae respiration rate at 20°C	d^{-1}	0.020	*H ovalis:* Longstaff and Dennison (1999) found biomass loss in 38 days of light deprivation (1/38 =0.026 d^{-1})
ϑ_{resp}^{MAC}	Arrhenius temperature scaling for respiration	-	1.08	
R_{mort}^{MAC}	Macroalgae mortality rate	d^{-1}	0.006	
S_{opt}^{MAC}	Lower salinity limit before increased mortality	ppt	9	*H ovalis:* Ralph (1998b) found no stress to photosynthesis @ 25% seawater and 150% seawater; Hillman (1985) found *H. ovalis* was able to grow in the range 10–45 ppt in SCE
S_{bep}^{MAC}	Magnitude of salinity effect on mortality rate	-	5	
S_{max}^{MAC}	Upper salinity limit before increased mortality	ppt	50	
$k_{biodrag}^{MAC}$	Coefficient of macrophyte biomass effect on drag	-	0.01	
k_{biotau}^{MAC}	Coefficient of macrophyte biomass effect on τ_0	N m^{-2} (g m^{-2})$^{-1}$	0.00125	*Assumed*
$\chi_{C:dw}^{MAC}$	Stoichiometry of C per unit dry weight (dw)	g g^{-1}	0.3	*H ovalis:* Hillman et al. (1995) Table 9 shows ~30% in SCE
$\chi_{C:N}^{MAC}$	Stoichiometry of C per N	mol C: mol N	22	*H ovalis:* Hillman et al. (1995)
$\chi_{C:N}^{MAC}$	Stoichiometry of N per P	mol C: mol N	17.5	*H ovalis:* Hillman et al. (1995)
c_Ω	Specific leaf area coefficient	m^2 mmol C^{-1}	0.00152	*H ovalis:* Baird et al. (2016) conversion 1.9 (m^2 gN^{-1}) * (14 gN molN^{-1}) * (1/17.5 molN molC^{-1})

4. Future development priorities

Bacteria, viruses and the microbial loop

The cycling of organic matter is complicated by microbial interactions between bacteria, micrograzers and viruses. The so-called "microbial loop" has been demonstrated to be an alternate "brown" pathway for trophic upscaling of detrital carbon, in contrast to the classically held model of the nutrient-phytoplankton-zooplankton "green" pathway (Li et al., 2014). The microbial loop assumes the micrograzers, made up of organisms such as heterotrophic nanoflagellates, exert a strong controlling force on bacterial abundance through predation, and influence rates of organic matter recycling by reducing bacteria available for mineralisation, and also through excretion of readily available nutrients. In fact Li et al., (2014) recently demonstrated the important role that the microbial loop plays in regulating the stoichiometry of food-web interactions, and highlighted that models that did not correctly parameterise this process may in fact lead to errors in the predicted level of N vs P limitation that algae may ultimately experience. Viral lysis of both heterotrophic organisms and photosynthetic organisms is also thought to considerably impact upon on food web nutrient recycling. For the most part the parameterisations introduced in the standard model approaches effectively "lump" these complex process into the net mortality rates that are applied (Li et al., 2013).

Within the SCE, Gedaria et al. (2013) presented a full year of data for bacteria and virus particle numbers along the length of the estuary for 2010, as determined by flow cytometry. These data highlight that bacterial numbers are indeed not constant, and vary considerably with season and region (Figure 9). Models accounting for bacteria and viral pools have been developed (Keller and Hood, 2011), however, are demanding of local data and rate estimates that are often not readily available. In the SCE, there remains limited information on small grazers such as protozoa and rotifers, making it difficult to fully configure and validate a dynamic model of the microbial loop.
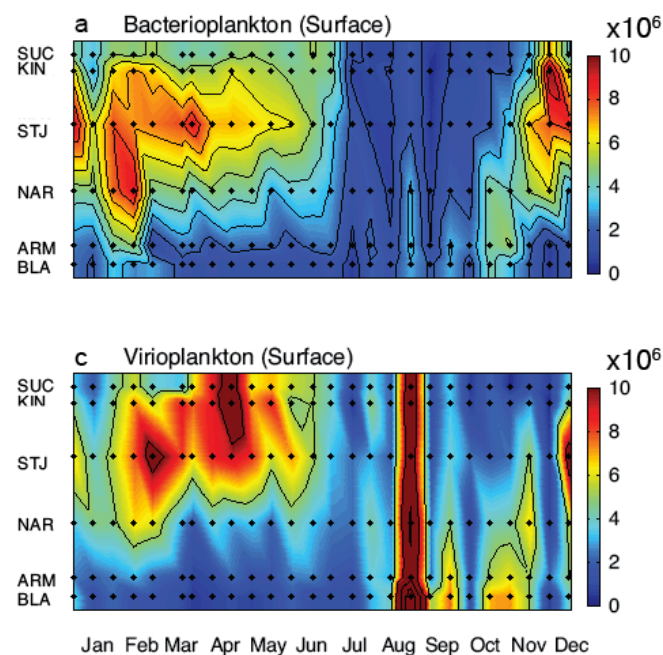

Figure 9. Field data demonstrating variability in bacteria (top) and virus-like particles (bottom) numbers (cells mL^{-1}; taken from Gedaria et al., 2013)

Benthic Invertebrates

It has been long recognised in the literature that benthic macroinvertebrates (BMI) have a complex effect on solute flux and redox boundaries via sediment particle mixing and burrowing activities. Along with these bioturbation activities other biological processes such as excretion can significantly affect the mineralisation of organic material, microbial processes and biological oxygen demand within the sediment. The impact on biogeochemical processes has been

demonstrated to differ among functional feeding groups of BMI's (Bartoli et al., 2009), however the diversity and activity of the BMI assemblage is strongly influenced seasonal changes in hydrodynamics (Braeckman et al., 2010), sediment characteristics (Levinton, 1972), and importantly the availability of oxygen (Mermillod-Blondin & Rosenberg, 2006). Prolonged hypoxic conditions can result in reduced activity and major shifts in BMI functional groups being dominated by a small number of opportunistic, hypoxic tolerant species (Wildsmith et al., 2011; Tweedley et al. 2016). In the SCE some data exists for bioturbation and biological processes of the differing functional groups (Pennifold & Davis, 2001), however, currently little is known about the nutrient flux rates associated with key BMI taxa or functional groups in the finer organic rich sediments of the upper estuary.

In order to provide improved parameterisation within the sediment digenesis model of the FABM-AED framework a series of bioturbation trials are being undertaken to measure nutrient flux rates for specific sediment "zones" of the upper and lower SCE, which will facilitate running the model according to the differing sediment attributes found throughout the estuary. These trials will provide sediment flux rates for the dissolved inorganic fractions, FRP, NO_x and NH_4, and organic nitrogen (DON) under steady state oxygen conditions (well oxygenated and hypoxia) as well as variable oxygen conditions (diurnal fluctuations between oxic and hypoxic conditions) for key functional groups (e.g., as represented by *Prionospio cirrifera*, *Arthritica semen* and *Capitella spp.*) and a more general BMI assemblage. This parameterisation of BMI effect on sediment biogeochemical processes will be an improvement on the commonly used biodiffusion coefficient D_B (Meysman et al., 2005) in sediment diagenesis models as it incorporates realistic and specific bioturbational behaviour of benthic fauna. A simple experiment assessing the sensitivity of 2 cm of biodiffusion and irrigation (as observed during laboratory trials) on the predictions of nutrient fluxes by the sediment diagenesis model CANDI-AED, setup as in Norlem et al. (2013), is shown in Figure 10.
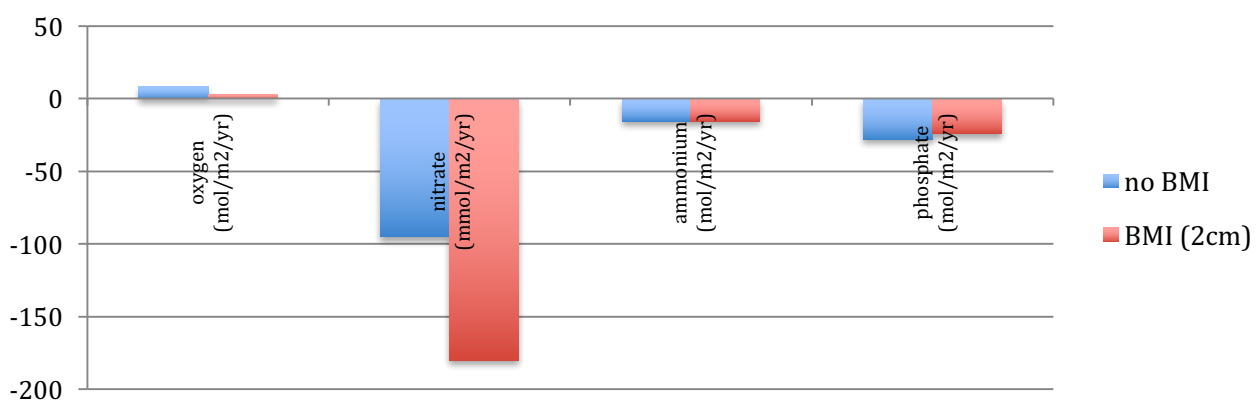

Figure 10. Sensitivity of nutrient flux predictions to benthic macroinvertebrate (BMI) effects within the top 2cm, as simulated with the sediment diagenesis model CANDI-AED.

Macroalgal biomass and wrack accumulation

Macroalgae are common in the SCE, including species such as *Gracilaria comosa*, *Chaetomorpha* and *Ulva flexuosa* and in shallow embayments of the lower portion of the domain (Astill & Lavery, 2001). Large blooms of macroalgae have been noted historically (since 1870) and the blooms have an important role on cycling of nutrients. Approaches to model macroalgae are similar as those described above for seagrasses, but usually they differ since they predominantly source their nutrients from the water column and may have more variable tissue nutrient stoichiometry. In addition, the need to simulate threshold shear stress that drives detachment of loosely attached macroalgal material is also important.

The accumulation of detached seagrass and macroalgal material (termed 'wrack') within shallow embayments and beaches has potential significance for both the biogeochemistry and ecology of the system, in addition to impacting the amenity of the estuary for fishing and recreation. However, approaches to model wrack formation and subsequent accumulation are in their infancy. Oldham et al. (2010) undertook an extensive analysis of wrack in Geographe Bay and identified basic characteristics of wrack, however model approaches to simulate wrack must be developed that are able to account for the changing reactivity of wrack from its origin and transport and accumulation on beaches. The Department of Transport are currently supporting research and development of such a model for the support or harbour management in WA (Hipsey et al., 2016b), and this will potentially be largely transferable to future versions of SCERM.

Zooplankton and jellyfish

It is known that both large and small zooplankton populations can play an important role in shaping estuary productivity and nutrient budgets. Additionally, they sit at the interface between lower trophic levels and biogeochemical processes and fish populations. Whilst methods for simulating zooplankton are well developed and available within the AED framework, unfortunately there is currently very limited data available for zooplankton in the SCE, including for micrograzers, macrograzers and jellyfish. This makes it challenging to configure and parameterise a dynamic model of zooplankton, and further monitoring and experimentation is therefore recommended in this area.

The two species of jellyfish medusae are common to the estuary, *Aurelia aurita* and *Phyllorhiza punctata*. These jellyfish form seasonal aggregations and are particularly common in summer when salinities exceed 25 ppt. Their absence in winter is explained by the flushing effect of winter rainfall and the low salinity (<10) and temperature (<20 °C) are below their tolerance limits (Rippingale and Kelly 1995). *A. aurita* may be able tolerate lower salinity and temperature than *P. puncata* (Groendahl, 1988). In winter, *P. punctata* is thought to survive as scyphistoma polyps in deeper water (Rippingale and Kelly 1995).

Although common to the estuary there is only limited information on the influence of these species on the estuary. Through the 1990's there were a number of student investigations undertaken at Curtin University. These investigations provide preliminary estimates of volumetric biomass of *P. punctata* medusae at 114, 073L (Parker, 1996). Estimates of oxygen production suggest maximum rates 0.024 mg mL^{-1} jellyfish hr^{-1} (equating to net production rates of up to 107 mg ind^{-1} d^{-1}), with rates affected by light availability and the size of the animal (Micin, 1989). Oxygen release is shown to be higher in the smaller medusae (Micin, 1989; Jafrii, 1997).

The release of dissolved organic carbon was also investigated in *P. punctata* taken from the Swan estuary, with estimated average DOC releases of 7.1 mg C medusa^{-1} hr^{-1}. (Firth, 1996). These are higher than those recorded for *A. aurita* – 1 mg C medusa^{-1} d^{-1}) and reflect the absence of the symbiotic zooxanthellae in that species (Hansson and Norman, 1995). DOC release rates in *P. punctata* are influenced by medusa size with estimates of between 5-19 μg C (mL of medusa)$^{-1}$ hr^{-1} (Firth, 1996), and other factors such as light and nutrient availability are also likely to influence the release of DOC.

Jellyfish can be voracious predators with evidence that *A. aurita* and *P. punctata* can influence mesozooplankton communities (Schneider and Behrends, 1998; Gueroun et al., 2015). Little is known of predation habits of these two jellyfish in the SCE, although there is some information to suggest that the ephyra and small medusa predate on rotifers and copepod nauplii, with the rate increasing with size (Jafri, 1997). Rates of *P. punctata* predation were 18 and 22 prey predator^{-1} hr^{-1} for rotifers and copepods, respectively.

Zooxanthellate jellyfish such as *P. punctata* may have potential to influence the estuarine environments through both top down (grazing) and bottom up (nutrient excretion; West et al., 2009). Local investigations by Jafri (1997) demonstrated a net release orthophosphate by *P. punctata* medusa during a small scale trial, with an average rate of 0.076 μg gwm^{-1} h^{-1} and an uptake of ammonia 0.109 μg gwm^{-1} h^{-1}.

The model CAEDYM (Chan et al., 2002; Hipsey & Hamilton, 2008) was originally extended to include the dynamics of jellyfish, *J*, with simple parameterisations for growth and respiration, summaried as:

$$\frac{dJ}{dt} = R_{Jmax} \underbrace{\Phi_{tem}^{JEL}(T)}_{\substack{\text{temperature} \\ \text{scaling}}} \underbrace{\Phi_{sal}^{JEL}(S)}_{\substack{\text{salinity} \\ \text{scaling}}} \underbrace{[f(POC) + f(I)]}_{\text{food \& light limitation}} - [R_{Jresp} - R_{Jexcr}]\Phi_{tem}^{JEL}(T) \tag{74}$$

where the food and limitation term assumes ingestion of organic material in parallel to nutrition of the medusae derived from the symbiotic algae, based on light. However, this model approach remains un-validated and has not been subsequently used due to lack of any data good in situ count data. Furthermore, the complication of jellyfish motility (both vertical and horizontal) makes the prospect of a validation complicated.

Therefore, whilst some indicative scenarios may be undertaken using the above data and standard approaches as a basis for model setup, further monitoring data and ongoing development is required to more completely assess the role of key zooplankton groups and jellyfish within the SCE modelling.

References

Adams, M.P., Hovey, R.K., Hipsey, M.R., Bruce, L.C., Ghisalberti, M., Lowe, R.J., Gruber, R.K., Ruiz-Montoya, L., Maxwell, P.S., Callaghan, D.P., Kendrick, G.A. and O'Brien, K. (2016) The seagrass-sediment-light feedback: where is it important? *Limnology and Oceanography* in press.

Adiyanti, S., Eyre, B.D., Maher, D.T., Santos, I., Golsby-Smith, L., Mangion, P. and Hipsey, M.R. (2016) Stable isotopes reduce parameter uncertainty of an estuarine carbon cycling model. *Environmental Modelling and Software* **79**, 233–255.

Adolf, J.E., Bachvaroff, T. and Place, A.R. (2008) Can cryptophytes trigger toxic *Karlodinium veneficum* blooms in eutrophic estuaries? *Harmful Algae* **8**, 119–128.

Adyel, T.M, Ocampo, C., Tareque, H., Oldham, C.E., Hipsey, M.R. (2015) Performance assessment of Wharf St Constructed Wetland 2009-2014. Cooperative Research Centre for Water Sensitive Cities, Melbourne, Australia.

Armengol, J., Caputo, L., Comerma, M., et al. (2003) Sau reservoir's light climate: relationships between Secchi depth and light extinction coefficient. *Limnetica* **22**, 195–210.

Astill, H.L. and Lavery, P.S. (2001) The dynamics of unattached benthic macroalgal accumulations in the Swan–Canning estuary. *Hydrological Processes* **15**, 2387–2399.

Baird, M.E., Adams, M.P., Babcock, R.C., et al. (2016) A biophysical representation of seagrass growth for application in a complex shallow-water biogeochemical model. *Ecological Modelling* **325**, 13–27.

Baklouti, M., Diaz, F., Pinazo, C., Faure, V. and Quéguiner, B. (2006) Investigation of mechanistic formulations depicting phytoplankton dynamics for models of marine pelagic ecosystems and description of a new model. *Progress in Oceanography* **71**, 1–33.

Bartoli, M., Vezzulli, L., Nizzoli, D., Azzoni, R., Porrello, S., Moreno, M., Viaroli, P. (2009) Short-term effect of oxic to anoxic transition on benthic microbial activity and solute fluxes in organic-rich phytotreatment ponds. *Hydrobiologia*, **629**(1), 123–136.

BMTWBM (2014) Hawkesbury-Nepean water quality modelling. Technical Report prepared for Sydney Water Corporation.

BMTWBM (2016) South-East Queensland estuary water quality modelling. Technical Report prepared for Healthy Waterways Partnership.

Braeckman, U., Provoost, P., Gribsholt, B., Van Gansbeke, D., Middelburg, J., Soetaert, K., Vanaverbeke, J. (2010) Role of macrofauna functional traits and density in biogeochemical fluxes and bioturbation. *Marine Ecology Progress Series*, **399**, 173–186.

Brearley, A. and Hodgkin, E. (2005) Ernest Hodgkin's Swanland: Estuaries and Coastal Lagoons of South-western Australia. University of Western Australia Press, Perth. 550pp.

Bruce, L.C., Cook, P.L.M. and Hipsey, M.R., 2011. Using a 3D hydrodynamic-biogeochemical model to compare estuarine nitrogen assimilation efficiency under anoxic and oxic conditions. In: Chan, F., Marinova, D. and Anderssen, R.S. (eds) *MODSIM2011, 19th International Congress on Modelling and Simulation.* Modelling and Simulation Society of Australia and New Zealand, December 2011, 3691–3697.

Bruce, L.C., Cook, P.L.M., Teakle, I. and Hipsey, M.R. (2014) Hydrodynamic controls on oxygen dynamics in a riverine salt-wedge estuary, the Yarra River estuary, Australia. *Hydrology and Earth System Sciences* **18,** 1397–1411.

Bruce, L.C., Cook, P.L.M and Hipsey, M.R., 2015. A model of oxygen and nitrogen biogeochemical response to hydrodynamic regimes in the Yarra River estuary. In: Weber, T., McPhee, M.J. and Anderssen, R.S. (eds) *MODSIM2015, 21st International Congress on Modelling and Simulation.* Modelling and Simulation Society of Australia and New Zealand, December 2015, 524–530.

Bruce, L.C., Hipsey, M.R. and Jones, N. (2016) Walcott Inlet and Collier Bay Biogeochemical Model. Unpublished Report for the WA Marine Science Institution, in preparation.

Bruggeman, J. and Bolding, K. (2014) A general framework for aquatic biogeochemical models. *Environmental Modelling and Software* **61**, 249–265.

Cerco, C.F. and Cole, T. (1993) Three-Dimensional Eutrophication Model of Chesapeake Bay. *Journal of Environmental Engineering* **119**, 1006–1025.

Cerco, C.F. and Moore, K. (2001) System-wide submerged aquatic vegetation model for Chesapeake Bay. *Estuaries* **24**, 522–534.

Chalker, B.E. (1980) Modeling light saturation curves for photosynthesis: An exponential function. *Journal of Theoretical Biology* **84**, 205–215.

Chan, T. Phytoplankton dynamics in a seasonal estuary. PhD Thesis from The University of Western Australia, Perth. 236pp.

Chan, T. and Hamilton, D.P. (2001) Effect of freshwater flow on the succession and biomass of phytoplankton in a seasonal estuary. *Marine and Freshwater Research* **52**, 869–884.

Chan, T., Hamilton, D.P., Robson, B., Hodges, B., Dallimore, C. (2002) Impacts of hydrological changes on phytoplankton succession in the Swan River, Western Australia. *Estuaries* **25**, 1406–1415.

Chao, X., Jia, Y., Shields, F.D., Wang, S.S.Y. and Cooper, C.M. (2010) Three-dimensional numerical simulation of water quality and sediment-associated processes with application to a Mississippi Delta lake. *Journal of Environmental Management*, **91**, 1456–1466.

Chung, S.W., Imberger, J., Hipsey, M.R. and Lee, H.S. (2014) The influence of physical and physiological processes on the spatial heterogeneity of a Microcystis bloom in a stratified reservoir. *Ecological Modelling* **289**, 133–149.

Cloern, J.E., Knowles, N., Brown, L.R., Cayan, D., Dettinger, M.D., Morgan, T.L., Schoellhamer, D.H., Stacey, M.T., van der Wegen, M., Wagner, R.W., Jassby, A.D. (2011). Projected Evolution of California's San Francisco Bay-Delta-River System in a Century of Climate Change. PLoS ONE **6**, e24465.

Crowe, S. A., Canfield, D. E., Mucci, A., Sundby, B. and Maranger, R. (2012) Anammox, denitrification and fixed-nitrogen removal in sediments from the Lower St. Lawrence Estuary. *Biogeosciences* **9**, 4309–4321.

del Barrio, P., Ganju, N.K., Aretxabaleta, A.L., Hayn, M., García, A. and Howarth, R.W. (2014) Modeling future scenarios of light attenuation and potential seagrass success in a eutrophic estuary. *Estuarine, Coastal and Shelf Science* **149**, 13–23.

Department of Parks and Wildlife (2015). Swan Canning River Protection Strategy. State Government of Western Australia

Devlin, M.J., Barry, J., Mills, D.K., Gowen, R.J., Foden, J., Sivyer, D. and Tett, P. (2008) Relationships between suspended particulate material, light attenuation and Secchi depth in UK marine waters. *Estuarine, Coastal and Shelf Science* **79**, 429–439.

Droop, M.R. (1974) The nutrient status of algal cells in continuous culture. *Journal of the Marine Biological Association of the United Kingdom* 54, 825–855.

Ebenhöh, W., Baretta-Bekker, J.G. and Baretta, J.W. (1997) The primary production module in the marine ecosystem model ERSEM II, with emphasis on the light forcing. *Journal of Sea Research* **38**, 173–193.

Firth, A. (1996) Mucus exudates of *Phyllorhiza punctate*: Dissolved organic carbon release in the Swan-Canning Estuary. Unpublished Biology Project 302 Report. School of Environmental Biology, Curtin University, Perth.

Fellman, J.B., Petrone, K.C. and Grierson, P.F. (2011) Source, biogeochemical cycling, and fluorescence characteristics of dissolved organic matter in an agro-urban estuary. *Limnology and Oceanography* **56**, 243–256.

Froelich, P.N. (1988) Kinetic control of dissolved phosphate in natural rivers and estuaries: A primer on the phosphate buffer mechanism. *Limnology and Oceanography* **33**, 649–668.

Forbes, V.R. and Kilminster, K. (2014) Monitoring seagrass extent and distribution in the Swan-Canning estuary. *Water Science Technical Series, Report no. 70*, Western Australia Department of Water, Perth Australia.

Gal, G., Hipsey, M.R., Parparov, A., Wagner, U., Makler, V. and Zohary, T. (2009) Implementation of ecological modeling as an effective management and investigation tool: Lake Kinneret as a case study. *Ecological Modelling* **220**, 1697–1718.

Gallegos, C. and Moore, K.A. (2000) Factors contributing to water-column light attenuation. pp. 16-27. In: Batiuk, R.A., Bergstrom, P., Kemp, W.M., Koch, E., Murray, L., Stevenson, J.C., Bartleson, R., Carter, V., Rybicki, N.B., Landwehr, J.M., Gallegos, C., Karrh, L., Naylor, M., Wilcox, D., Moore, K.A., Ailstock, S. and Teichberg, M. (eds.), Chesapeake Bay Submerged Aquatic Vegetation Water Quality and Habitat-based Requirements and Restoration Targets: A Second Technical Synthesis. U.S. Environmental Protection Agency, Chesapeake Bay Program, Annapolis, Maryland.

Gallegos, C.L. (2001) Calculating optical water quality targets to restore and protect submersed aquatic vegetation: overcoming problems in partitioning the diffuse attenuation coefficient for Photosynthetically Active Radiation. *Estuaries* **24**, 381–397.

Gedaria, A.I., Paparini, A. and Hipsey, M.R. (2013) Integration of cytometric, bio-molecular and nutrient data to explore microbial dynamics in the Swan River Estuary. University of Western Australia Technical Report prepared for the Swan River Trust, Perth, Australia. 94pp.

Gillibrand, P.A., Andrewartha, J.R. and Herzfeld, M. (2012) Numerical Hydrodynamic Modelling of the Leschenault Estuary. CSIRO Technical Report. 79pp.

Griffin, S.L., Herzfeld, M. and Hamilton, D.P. (2001) Modelling the impact of zooplankton grazing on the phytoplankton biomass during a dinoflagellate bloom in the Swan River estuary, Western Australia. *Ecological Engineering* **16**, 373–394.

Gröndahl, F. (1988) A comparative ecological study on the scyphozoans Aurelia aurita, Cyanea capillata and C. lamarckii in the Gullmar Fjord, western Sweden, 1982 to 1986. *Marine Biology* **97**, 541–550.

Gueroun, Sh.M., Yahia, O.K.D., Deidun, A., Fuentes, V., Piraino, S., Uyahia, M.N.D. (2015) First record and potential tropic impact of *Phyllorihiza punctate* (Cnidaria: Scyphozoa) along the north Tunisian coast (South Western Mediterranean Sea). *Italian Jounal of Zoology* **82**, 95-100.

Hallegraeff, G.M., Mooney, B. and Evans, K. (2011) What triggers *Karlodinium veneficum* blooms in the Swan Canning River systems? Final Report for the Swan Canning Research and Innovation Program project no. RSG09TAS01, University of Tasmania, Hobart, Australia.

Hamilton, D.P., Douglas, G.B., Adeney, J.A. and Radke, L.C. (2006) Seasonal changes in major ions, nutrients and chlorophyll a at two sites in the Swan River estuary, Western Australia. *Marine and Freshwater Research* **57**, 803–815.

Hamilton D.P., Schladow, S.G. (1997) Prediction of water quality in lakes and reservoirs. Part 1 – Model description. *Ecological Modelling* **96**, 91–110.

Hansson, L.J. and Norman, B. (1995) Release of dissolved organic carbon (DOC) by the scyphozoan jellyfish, *Aurelia auritia* and its potential influence on the production of planktic bacteria. *Marine Biology* **121**, 527–532.

Harvey, H.R., and Mannino, A. (2001) The chemical composition and cycling of particulate and macromolecular dissolved organic matter in temperate estuaries as revealed by molecular organic tracers. *Organic Geochemistry* **32**, 527–542.

Herzfeld, M., Jones, E., Margvelashvili, N., et al. (2014) SEQ RWQM V3 Phase II Final Report. CSIRO report to Health Waterways Partnership. 170 pp.

Hillman, K. (1985) The production ecology of the seagrass *Halophila ovalis* (R. Br.) Hook, in the Swan/Canning Estuary, Western Australia. Ph.D. dissertation, Botany Department, The University of Western Australia, 333p.

Hillman, K., McComb, A.J. and Walker, D.I. (1995) The distribution, biomass and primary production of the seagrass *Halophila ovalis* in the Swan/Canning Estuary, Western Australia. *Aquatic Botany* **51**, 1–54.

Hipsey, M.R., Kilminster, K. and Busch B. (2016a). The Swan-Canning Estuary Response Model (SCERM) v1: Model validation and performance assessment. AED Report #R29, The University of Western Australia, Perth, Australia. 49pp.

Hipsey, M.R., Bruce, L. and Oldham C. (2016b). Modelling coastal wrack dynamics: Model requirements & development approach. AED Report #R30, The University of Western Australia, Perth, Australia. 22pp.

Hipsey, M.R., Salmon, S.U., Aldrige, K.T. and Brookes, J.D. (2010) Impact of hydro-climatological change and flow regulation on physical and biogeochemical dynamics of the Lower River Murray, Australia. *8th International Symposium on Ecohydraulics (ISE2010)*, September, 2010, Korea.

Hipsey, M.R., Antenucci, J.P. and Brookes, J.D. (2008) A generic, process-based model of microbial pollution in aquatic systems. *Water Resources Research* **44**, W07408.

Hipsey, M.R., Bruce, L.C. and Kilminster, K. (2013) A 3D hydrodynamic-biogeochemical model for assessing artificial oxygenation in a riverine salt-wedge estuary. In: Piantadosi, J., Anderssen, R.S. and Boland J. (eds) MODSIM2013, 20th International Congress on Modelling and Simulation. Modelling and Simulation Society of Australia and New Zealand, December 2013, pp. 1770–1776

Hipsey, M.R., Busch, B.D. (2012) Lower Lakes water quality recovery dynamics. *University of Western Australia Technical Report prepared for South Australian Department of Environment and Natural Resources*, Adelaide, Australia. 81pp.

Hipsey, M.R. and Hamilton, D.P. (2008) Computational Aquatic Ecosystem Dynamic Model: CAEDYM v3 Science Manual. Centre for Water Research Report, 140pp.

Hipsey, M.R., Kilminster, K., Busch, B.D., Bruce, L.C. and Larsen, S. (2014a) Modelling oxygen dynamics in the Upper Swan estuary and Canning Weir Pool. AED Report #R25 prepared for the Department of Water, The University of Western Australia, Perth, Australia. 99pp.

Hipsey, M.R., Salmon, S.U. and Mosley, L.M. (2014b) A three-dimensional hydro-geochemical model to assess lake acidification risk. *Environmental Modelling and Software* **61**, 433–457.

Hodgkin E.P. (1987) The Hydrology of the Swan River Estuary: Salinity the Ecological Master Factor. In: The Swan River Estuary Ecology and Management (Ed. John, J.), 34–44p. Curtin University of Technology, Bentley, Western Australia.

Jafri. A.W. (1997) Life History and Energy Relations of *Phyllorhiza punctata* (Cnidaria: Rhizostomae). Masters Thesis, Curtin University.

Jassby, A.T. and Platt, T. (1976) Mathematical formulation of the relationship between photosynthesis and light for phytoplankton. *Limnology and Oceanography* **21**, 540–547.

Jeffrey, S.W. (1981) An improved thin-layer chromatographic technique for marine phytoplankton pigments. *Limnology and Oceanography* **26**, 191–197.

Jellison, R. and Melack, J. (1993) Meromixis and vertical diffusivities in hypersaline Mono Lake, California. *Limnology and Oceanography* **38**, 1008–1019.

Keller, D.P. and Hood, R.R. (2011) Modeling the seasonal autochthonous sources of dissolved organic carbon and nitrogen in the upper Chesapeake Bay. *Ecological Modelling* **222**, 1139–1162.

Kim, D.-K., Zhang, W., Hiriart-Baer, V., Wellen, C., Long, T., Boyd, D. and Arhonditsis, G.B. (2014) Towards the development of integrated modelling systems in aquatic biogeochemistry: a Bayesian approach. *Journal of Great Lakes Research* **40**, 73–87.

Kirk, J.T.O. (1994). Light and Photosynthesis in Aquatic Ecosystems, 2nd ed. Cambridge University Press.

Kostoglidis, A., Pattiaratchi, C.B. and Hamilton, D.P. (2005) CDOM and its contribution to the underwater light climate of a shallow, microtidal estuary in south-western Australia. *Estuarine Coastal Shelf Science* **63**, 469–477.

Lavery, P.S., Oldham, C.E. and Ghisalberti, M. (2001) The use of Fick's First Law for predicting porewater nutrient fluxes under diffusive conditions. *Hydrological Processes* **15**, 2435–2451.

Lee, S.B. and Birch, G.F. (2012) Utilising monitoring and modelling of estuarine environments to investigate catchment conditions responsible for stratification events in a typically well-mixed urbanised estuary. *Estuarine, Coastal and Shelf Science* **111**, 1–16.

Levinton, J. (1972). Stability and trophic structure in deposit-feeding and suspension-feeding communities. *The American Naturalist* **106**, 472–486.

Li, Y., Waite, A.M., Gal, G. and Hipsey, M.R. (2013) An analysis of the relationship between phytoplankton internal stoichiometry and water column N:P ratios in a dynamic lake environment. *Ecological Modelling* **252**, 196–213.

Li, Y., Gal, G., Makler-Pick, V., Waite, A.M., Bruce, L.C. and Hipsey, M.R. (2014) Examination of the role of the microbial loop in regulating lake nutrient stoichiometry and phytoplankton dynamics. *Biogeosciences* **11**, 2939–2960.

Los, F.J. and Wijsman, J.W.M. (2007) Application of a validated primary production model (BLOOM) as a screening tool for marine, coastal and transitional waters. *Journal of Marine Systems* **64**, 201–215.

Marti, C.L. and Imberger, J. (2015) A real-time management system for the Perth Coastal Margin, Western Australia. *Proceedings of the 36th IAHR World Congress*, The Hague, The Netherlands. 10pp.

Mermillod-Blondin, F., & Rosenberg, R. (2006). Ecosystem engineering: the impact of bioturbation on biogeochemical processes in marine and freshwater benthic habitats. *Aquatic Sciences*, *68*(4), 434–442. http://doi.org/10.1007/s00027-006-0858-x

Meysman, F.J.R., Boudreau, B.P. and Middelburg, J.J. (2005). Modeling reactive transport in sediments subject to bioturbation and compaction. *Geochimica et Cosmochimica Acta* **69**, 3601–3617.

Micin, S. (1989). Factors affecting productivity of *Phyllorhiza punctata* in the Swan Canning Estuary. Unpublished Biology Project 302 Report. School of Environmental Biology, Curtin University, Perth, Western Australia.

Monod, J. (1950). La technique de culture continue; theorie et applications. *Annales de l'Institut Pasteur* **79**, 390–410.

Mooney, B.D., Hallegraeff, G.M. and Place, A.R. (2010) Ichthyotoxicity of four species of gymnodinioid dinoflagellates (Kareniaceae, Dinophyta) and purified karlotoxins to larval sheepshead minnow. *Harmful Algae* **9**, 557–562.

Norlem, M., Paraska, D. and Hipsey, M.R. (2013) Sediment-water oxygen and nutrient fluxes in a hypoxic estuary. In: Piantadosi, J., Anderssen, R.S. and Boland J. (eds) *MODSIM2013, 20th International Congress on Modelling and Simulation*. Modelling and Simulation Society of Australia and New Zealand, December 2013, pp. 1777–1783.

Oldham et al. (2010)

Paraska, D.W., Hipsey, M.R. and Salmon, S.U. (2014) Sediment diagenesis models: Review of approaches, challenges and opportunities. *Environmental Modelling and Software* **61**, 297–325.

Parker, J (1996). Biomass of *Phyllorhiza punctata* in the Swan-Canning estuary in the Summer 1995-96. Unpublished Biology Project 302 Report. School of Environmental Biology, Curtin University, Perth, Western Australia.

Pennifold, M. and Davis, J. (2001) Macrofauna and nutrient cycling in the Swan River Estuary, Western Australia: experimental results. *Hydrological Processes* **15**, 2537–2553.

Petrone, K.C. 2010. Catchment export of carbon, nitrogen, and phosphorus across an agro-urban land use gradient, Swan-Canning River system, southwestern Australia. *Journal of Geophysical Research (Biogeosciences)*, 115.

Petrone, K.C., Fellman, J.B., Hood, E., Donn, M.J. and Grierson, P.F. (2011). The origin and function of dissolved organic matter in agro-urban coastal streams, *Journal of Geophysical Research: Biogeosciences* **116**(G1), G01028.

Petrone, K.C., Richards, J.S., Grierson, P.F. (2009) Bioavailability and composition of dissolved organic carbon and nitrogen in a near coastal catchment of south-western Australia. *Biogeochemistry* **92**, 27–40.

Ralph, P.J. (1998a) Photosynthetic response of laboratory-cultured *Halophila ovalis* to thermal stress, *Marine Ecology Progress Series* **171**, 123–130.

Ralph, P.J. (1998b) Photosynthetic responses of *Halophila ovalis* (R. Br.) Hook. f. to osmotic stress. *Journal of Experimental Marine Biology and Ecology* **227**, 203–220.

Ralph, P.J. and Burchett, M.D. (1995). Photosynthetic responses of the seagrass *Halophila ovalis* (R. Br.) Hook. f. to high irradiance stress, using chlorophyll a fluorescence. *Aquatic Botany* **51**, 55–66.

Riley, J.P. & Skirrow, G. (1974) Chemical Oceanography. Academic Press, London.

Rippingale, R.J. and Kelly, S.J. (1995) Reproduction and survival of Phyllorhiza punctata (Cnidaria: Rhizostomeae) in a seasonally fluctuating salinity regime in Western Australia. *Marine and Freshwater Research* **46**, 1145–1151.

Rhee, G.Y. and Gotham, E.J. (1981) The effect of environmental factors on phytoplankton growth: temperature and the interactions of temperature with nutrient limitation. *Limnology and Oceanography* **26**, 635–648.

Roberts, K. L., V. M. Eate, B. D. Eyre, D. P. Holland, and P. L. M. Cook. 2012. Hypoxic events stimulate nitrogen recycling in a shallow salt-wedge estuary: The Yarra River Estuary, Australia. *Limnology and Oceanography*, 57: 1427–1442.

Robson, B.J. and Hamilton, D.P. (2003) Summer flow event induces a cyanobacterial bloom in a seasonal Western Australian estuary. *Marine and Freshwater Research* **54**, 139–151.

Robson, B.J., Hamilton, D.P. (2004) Three-dimensional modelling of a *Microcystis* bloom event in the Swan River estuary, Western Australia. *Ecological Modelling* **174**, 203–222.

Robson, B.J., Bukaveckas, P.A. and Hamilton, D.P. (2008). Modelling and mass balance assessments of nutrient retention in a seasonally flowing estuary (Swan River Estuary, Western Australia). *Estuarine Coastal and Shelf Science* **76**, 282–292.

Robson, B., Webster, I., Rosebrock, U. (2006) Biogeochemical modelling and nitrogen budgets for the Fitzroy Estuary and Keppel Bay. Cooperative Research Centre for Coastal Zone, Estuary & Waterway Management Technical Report 40 CRC for Coastal Zone, Estuary & Waterway Management.

Romero, J.R., Antenucci, J.P. and Imberger, J. (2004) One- and three-dimensional biogeochemical simulations of two differing reservoirs. *Ecological Modelling* **174**, 143–160.

Ruibal-Conti, A.L., Ocampo, C., Adyel, T.M., Hipsey, M.R. and Oldham, C.E. (2015) Performance assessment the of Anvil Way Compensation Basin living stream: 2004–2013. Cooperative Research Centre for Water Sensitive Cities, Perth, Australia.

Salmon *et al.* (2014)

Sarthou, G., Timmermans, K.R., Blain, S. and Tréguer, P. (2005) Growth physiology and fate of diatoms in the ocean: a review. *Journal of Sea Research* **53**, 25–42.

Schneider, G & Behrends, G. (1998). Top-down control in a neritic plankton system by *Aurelia aurita* medusa – A summary. *Ophelia* **48**, 71–82.

Shimoda, Y., Arhonditsis, G.B. 2016. Phytoplankton functional type modelling: running before we can walk? A critical evaluation of the current state of knowledge. *Ecological Modelling* **320**, 29–43.

Smith, C.S., Haese, R.R. and Evans, S. (2010) Oxygen demand and nutrient release from sediments in the upper Swan River estuary. Geoscience Australia Record, 2010/28. Commonwealth Government, Canberra.

Smith, C.S., Murray, E.J., Hepplewhite, C. and Haese, R.R. (2007) Sediment water interactions in the Swan River estuary: Findings and management implications from benthic nutrient flux surveys, 2000-2006. Geoscience Australia Record 2007/13. Commonwealth Government, Canberra.

Steele, J.H. (1962) Environmental control of photosynthesis in the sea. *Limnology and Oceanography* **7**, 137–150.

Sundareshwar, P.V. and Morris, J.T. (1999) Phosphorus sorption characteristics of intertidal marsh sediments along an estuarine salinity gradient. *Limnology and Oceanography* **44**, 1693–1701.

Talling, J.F. (1957) The phytoplankton population as a compound photosynthetic system. *New Phytologist* **56**, 133–149.

Testa, J.M., Brady, D.C., Di Toro, D.M., Boynton, W.R., Cornwell, J.C. and Kemp, W.M. (2013) Sediment flux modeling: Simulating nitrogen, phosphorus, and silica cycles. *Estuarine Coastal and Shelf Science* **131**, 245–263.

Testa, J.M., Li, Y., Lee, Y.J., Li, M., Brady, D.C., Di Toro, D.M., Kemp, W.M. and Fitzpatrick, J.J. (2014) Quantifying the effects of nutrient loading on dissolved O_2 cycling and hypoxia in Chesapeake Bay using a coupled hydrodynamic–biogeochemical model. *Journal of Marine Systems* **139**, 139–158.

Thompson, P.A. (1998) Spatial and temporal patterns of factors influencing phytoplankton in a salt wedge estuary, the Swan River, Western Australia. *Estuaries* **21**, 801–817.

Thompson, P.A. and Hosja, W. (1996) Nutrient limitation of phytoplankton in the Upper Swan River Estuary, Western Australia. *Marine and Freshwater Research* **47**,659–667.

Tweedley, J.R., Hallett, C.S., Warwick, R.M., Clarke, K.R. and Potter, I.C. (2016) The hypoxia that developed in a microtidal estuary following an extreme storm produced dramatic changes in the benthos. *Marine and Freshwater Research* **67**, 327–341.

Waltham, N.J., Barry, M., McAlister, T., Weber, T. and Groth, D. (2014) Protecting the Green Behind the Gold: Catchment-Wide Restoration Efforts Necessary to Achieve Nutrient and Sediment Load Reduction Targets in Gold Coast City, Australia. *Environmental Management* **54**, 840–851.

Wanninkhof, R. (1992) Relationship between windspeed and gas exchange over the ocean. *Journal of Geophysical Research (Oceans),* **97**(C5), 7373–7382.

Wanninkhof, R. and McGillis, W.R. (1999) A cubic relationship between air-sea CO2 exchange and wind speed. *Geophysical Research Letters* **26**, 1889–1892.

Webb, W.L., Newton, M. and Starr, D. (1974) Carbon dioxide exchange of *Alnus rubra*: a mathematical model. *Oecologia* **17**, 281–291.

Weiss, R. (1974) Carbon dioxide in water and seawater: the solubility of a non-ideal gas. *Marine Chemistry* **2**, 203–215.

West, E.J., Pitt, K.A., Welsh, D.T. Koop, K and Rissik (2009) Top-down and bottom-up influences of jellyfish on primary productivity and planktonic assemblages. *Limnology and Oceanography* **54**, 2058–2071.

Wild-Allen, K., Herzfeld, M., Thompson, P.A., Rosebrock, U., Parslow, J. and Volkman, J.K. (2010) Applied coastal biogeochemical modelling to quantify the environmental impact of fish farm nutrients and inform managers. *Journal of Marine Systems* **81**, 134–147.

Wild-Allen, K., Skerratt, J., Whitehead, J., Rizwi, F. and Parslow, J. (2013) Mechanisms driving estuarine water quality: A 3D biogeochemical model for informed management. *Estuarine, Coastal and Shelf Science* **135**, 33–45.

Wildsmith, M.D., Rose, T.H., Potter, I.C., Warwick, R.M. and Clarke, K.R. (2011) Benthic macroinvertebrates as indicators of environmental deterioration in a large microtidal estuary. *Marine Pollution Bulletin*, 62: 525–538.

Vähätalo, A.V., Salkinoja-Salonen, M., Taalas, P. and Salonen, K. (2000) Spectrum of the quantum yield for photochemical mineralization of dissolved organic carbon in a humic lake. *Limnology and Oceanography* **45**, 664–676.

Vähätalo, A.V. and Zepp, R.G. (2005) Photochemical Mineralization of Dissolved Organic Nitrogen to Ammonium in the Baltic Sea. *Environmental Science and Technology* **39**, 6985–6992.

Valchon, D. and Prairie, Y.T. (2013) The ecosystem size and shape dependence of gas transfer velocity versus wind speed relationships in lakes. *Canadian Journal of Fisheries and Aquatic Sciences* **70**, 1757–1764.

Vilhena, L.C. (2013) Physical-biological coupling in aquatic ecosystems: the role of hydrodynamics in structuring phytoplankton communities. PhD Thesis, Centre for Water Research, The University of Western Australia, Perth, Australia. 146pp.

Yakushev, E.V., Protsenko, E.A., Bruggeman, J., Bellerby, R.G.J., Pakhomova, S.V., Couture, R.-M., and Yakubov, S. (2016) Bottom RedOx Model (BROM, v.1.0): a coupled benthic-pelagic model for simulation of seasonal anoxia and its impact. *Geoscientific. Model Development Discussions*, in review.

Zhang, W., Faulkner, J.W., Giri, S.K., Geohring, L.D. and Steenhuis, T.S. (2009) Evaluation of two Langmuir models for phosphorus sorption of phosphorus-enriched soils in New York for environmental applications. *Soil Science* **174**, 523–530.

Zhu, Y., Hipsey, M.R., McCowan, A., Beardall, J. and Cook, P.L.M. (2016) The role of bioirrigation in sediment phosphorus dynamics and blooms of toxic cyanobacteria in a temperate lagoon. *Environmental Modelling & Software*, **86**, 277-304.